Journal of Catalysis 312 (2014) 123–138

Contents lists available at ScienceDirect

Journal of Catalysis

journal homepage: www.elsevier.com/locate/jcat

Tailoring of the structure of Fe-cationic species in Fe-ZSM-5 by distribution of Al atoms in the framework for N_2O decomposition and NH_3-SCR-NO_x

Petr Sazama *, Blanka Wichterlová, Edyta Tábor, Petr Šťastný, Naveen K. Sathu, Zdeněk Sobalík, Jiří Dědeček, Štěpán Sklenák, Petr Klein, Alena Vondrová

J. Heyrovský Institute of Physical Chemistry, Academy of Sciences of the Czech Republic, CZ-182 23 Prague 8, Czech Republic

ARTICLE INFO

Article history:
Received 18 October 2013
Revised 22 January 2014
Accepted 28 January 2014
Available online 21 February 2014

Keywords:
Fe-ZSM-5 zeolite
Structure of Fe species
Fe(III)-oxo species
Al distribution in the framework
Mössbauer spectroscopy
UV–Vis
H_2-TPR
N_2O decomposition
NH_3-SCR-NO

ABSTRACT

The heterogeneity and redox behavior of Fe-cationic species in Fe-ZSM-5 catalysts for N_2O decomposition and NH_3-SCR-NO_x were analyzed by Mössbauer and UV–Vis spectroscopy, TPR-H_2, and reaction kinetic measurements. Iron was introduced into ZSM-5 zeolites of similar Si/Al but with different populations of close (Al–Si–Si–Al sequences in one ring – Al pairs) and far distant (single Al in different rings) Al atoms in the zeolite framework. It has been found that Al pairs in 6MRs of the framework greatly stabilize divalence of bare Fe(II) ions and $[Fe(II)–O–Fe(II)]^{2+}$ complexes even in oxidizing atmosphere. These species were completely oxidized only with N_2O and recognized as the most active sites in N_2O decomposition. On the contrary, the prevailing concentration of single Al atoms resulted at comparable conditions in high population of Fe(III)-oxo species. Fe(III)-oxo species of low nuclearity with partially compensated positive charge by the zeolite framework facilitate the formation of highly active oxygen species in an O_2-containing atmosphere and are the most active sites in NH_3-SCR-NO_x. These findings show that manipulation of the structure of Fe-cationic species can be achieved by the synthesis of zeolites with different distributions of Al atoms between Al pairs and single Al atoms in the framework. This represents a potential for tailoring of catalytic properties of Fe-zeolite based catalysts for abatement of nitrogen oxides.

1. Introduction

Since the pioneering works of Panov et al. [1] and Uddin et al. [2], it has been well established that iron zeolites are among the most active catalysts for the decomposition of N_2O to O_2 and N_2 and selective catalytic reduction of nitrogen oxides by ammonia (NH_3-SCR-NO_x, (NO/NO_2)). In the last two decades, considerable effort has been expended in analysis of the structure and function of Fe species [3–8], the mechanism of the above reactions [9–12] as well as methods of preparing the respective active sites in iron zeolites [7,8,13,14]. The structural analysis of Fe species in Si-rich Fe-zeolites with MFI, FER, and BEA* topology of unique redox activity in reactions of N_2O decomposition [15–17], and SCR-NO_x by ammonia [14,18–22], demonstrated that Fe can be found in a diverse set of oxidation states and stereochemical conformations.

Analysis of the relationship between the structure and activity of (Si-rich) Fe-zeolites has been continuously faced by the problem associated with preparing samples containing one highly predominant type of Fe species. The main reason for this lies in the fact that both Fe(II) and Fe(III) ions exhibit a high tendency to hydrolyze at pH > 4 [23] during Fe ion-exchange. Consequently, Fe-zeolite samples mostly contain both single Fe ions and various Fe(III)-oxo species ranging from di- and polynuclear counter-ion species up to oligomeric entities and small Fe oxide particles as observed in spectral studies (e.g. in [7,24–26]) and providing their semi-quantitative analysis. It was concluded that at very low Fe loadings (Fe/Al < 0.1), predominantly single Fe ions are present in cationic sites and with increasing Fe concentration, di- and polynuclear Fe(III)-oxo species are incorporated, followed by small oxide particles. There is a consensus that the Fe sites responsible for the activity in SCR-NO_x and N_2O decomposition are ion-exchanged Fe-oxo species, and oligomeric Fe species can play the role of active centers for NO_x or N_2O conversion only at high temperatures [7,27]. The most active sites for N_2O decomposition were suggested to be isolated bare Fe ions [16,26,28–33] or dinuclear Fe(II)-oxo species [34–36] in cationic sites. Isolated Fe ions [27,37] and dinuclear Fe-oxo species [3,38] in cationic sites were

* Corresponding author.
E-mail address: petr.sazama@jh-inst.cas.cz (P. Sazama).

http://dx.doi.org/10.1016/j.jcat.2014.01.019
0021-9517/

also suggested as the active sites for NH_3-SCR-NO_x. However, the structure and nuclearity of the ion-exchanged Fe-oxo species remains a subject of discussion. The Fe-Fe distance of 3.05 Å in Fe-ZSM-5 (Fe/Al ~ 1) obtained in EXAFS studies [39,40], and similar Mössbauer parameters of Fe-zeolites and Fe-oxo complexes of methane monooxygenase [24,41–43] are consistent with the presence of dinuclear oxo-bridged or di-oxo-bridged Fe species. However, the coordination and redox state of counter-ion Fe-oxo species are highly versatile and depend strongly on the Fe-zeolite pre-treatment [39,41], temperature, and composition of the reactant mixtures [26,40,44–47]. Understanding of the structure, these counter-ion species and the critical conditions for their formation represent key parameters for tailored synthesis of Fe-zeolite catalysts with optimized catalytic properties.

During N_2O decomposition, the Fe(II) ions in the cationic sites immediately react with N_2O to form molecular nitrogen and the so-called α-oxygen bound to the original Fe(II) ion [1,15,16] or a dinuclear Fe(II)-oxo complex [48,49]. While the recombination of two anion radicals in Fe-zeolites is a slow process, these readily interact with an additional N_2O molecule from the gas phase, resulting in the formation of di-nitrogen and di-oxygen. The overall N_2O decomposition can be described in simplified terms as follows:

$$\mathrm{Fe(II)} + \mathrm{N_2O} \rightarrow \mathrm{Fe(III)O^-} + \mathrm{N_2} \quad \text{fast} \tag{1}$$

$$\mathrm{Fe(III)—O^-} + \mathrm{N_2O} \rightarrow \mathrm{Fe(II)} + \mathrm{O_2} + \mathrm{N_2} \quad \text{medium} \tag{2}$$

$$\mathrm{2Fe(III)—O^-} \rightarrow \mathrm{2Fe(II)} + \mathrm{O_2} \quad \text{slow} \tag{3}$$

The Fe(III)-oxo species were suggested to be the active sites in the reduction of NO_x by ammonia [50], based on the Fe(III)–Fe(II) redox process, described by the simplified reaction steps (4) and (5):

$$\mathrm{Fe(III)—O_2—Fe(III)} + \mathrm{NO} \rightarrow \mathrm{Fe(II)—O—Fe(II)} + \mathrm{NO_2} \tag{4}$$

$$\mathrm{Fe(III)—O_2—Fe(III)} + \mathrm{2NO_2} + \mathrm{2NH_3} \rightarrow \mathrm{Fe(II)—O—Fe(II)} + \mathrm{2N_2} + \mathrm{O_2} + \mathrm{3H_2O} \tag{5}$$

$$\mathrm{Fe(II)—O—Fe(II)} + \mathrm{1/2O_2} \rightarrow \mathrm{Fe(III)—O_2—Fe(III)} \tag{6}$$

It follows that the structure of the active Fe sites for the N_2O decomposition and NH_3-SCR-NO_x transformation would require the opposite Fe redox cycles. Nevertheless, the activities in both the reactions are exclusively connected with the exchanged Fe species charge balanced by the zeolite negative framework, and not with any "supported" Fe. Moreover, as the Fe species are active only if charge balanced in Si-rich zeolites exhibiting low Al concentrations in the framework, and not in Al-rich faujasites (Si/Al < 3), their structure should be connected with the distribution of the Al atoms in these zeolites, i.e. the distribution of the local negative charge in the framework. Consequently, the present study attempts to analyze the structures of the Fe sites in ZSM-5 with their surroundings, i.e. oxygen ligands bearing negative charges of the framework AlO_4^- atoms.

The low concentration of Al in the framework of ZSM-5 zeolites (Si/Al > 12), and Si-rich zeolites in general, inducing different local negative charges, emphasizes the importance of the distribution of Al atoms in the framework for balancing the charges of various metal species [26,51]. The reported attempt to correlate the structure of the Fe species estimated from UV–Vis MLCT transitions with the calculated statistical distribution of Al atoms in the framework can hardly be generally justified. Analysis of a large number of Si-rich zeolite samples (MFI, FER, BEA*, MWW) makes possible to state that the distribution of Al atoms in their framework is not random and not controlled by statistics, but by the conditions of the zeolite synthesis. This is in agreement with the fact that the hydrothermal synthesis of zeolites is a process controlled kinetically and not by thermodynamics [52]. We have demonstrated that the Al–Si–Al sequences do not occur in Si-rich zeolites for compositions with Si/Al > 12, but the presence of Na^+ ions and polarization of TPA^+ by anions decisively affects the formation of far distant single Al atoms located in different rings and Al pairs (Al–Si–Si–Al sequences) in one ring of the framework, respectively [51,53,54]. Al pairs in ZSM-5 have been found in 6MRs of cationic sites predominantly populated in β rings (60–80%), less in α rings (10–40%), while γ rings have very low populations below 10% (see Fig. 1 and for details Refs. [51,55]). These conclusions are based on analysis of the Co(II) ion-exchange capacity in hydrated zeolites, bare Co(II) ions in dehydrated Co-zeolites monitored by d–d transitions in the Vis spectra, and ^{27}Al and ^{29}Si MAS NMR analysis, described in detail in Refs. [51,54,56–59]. In the laboratory synthesis, the variation in the relative concentration of Al atoms in Al pairs can be extended from 5% to 85% in ZSM-5, with the opposite trend for single Al atoms. We have also found substantial differences (up to 80 rel.%) in the relative concentrations of Al atoms in Al pairs in commercial ZSM-5 samples of similar Si/Al composition, particularly with Si/Al between 12 and 30 [56].

These findings emphasize the importance of analysis of the distribution of Al atoms in the framework of parent zeolites before using them to prepare metal-zeolite catalysts, but at the same time rises up questions if the structure of metal sites is affected by the distribution of AlO_4^- negative charges in the framework of high-silica zeolites. In the present study, we investigated the governance of the distribution of Al atoms in the framework of ZSM-5 for the structure, redox behavior, and function of the Fe species in ZSM-5 zeolites in N_2O decomposition and NH_3-SCR-NO_x. For this purpose, we selected three samples of ZSM-5 of similar Si/Al composition, but basically differing in the distribution of Al atoms in the framework between Al pairs and single Al atoms. Each of these zeolites was exchanged with Fe ions of increasing concentration ranging from 0.39 to 4.6 wt.%, representing an Fe/Al range of 0.06–0.82 suitable for analysis of active sites for both the N_2O decomposition and NH_3-SCR-NO_x. We anticipate that understanding of the effect of the distribution of Al atoms in the framework on the structure and redox behavior of Fe sites will enable tailoring the individual Fe species and their population in ZSM-5 zeolites.

2. Experimental

2.1. Parent ZSM-5 zeolites

Analysis of the effect of the distribution of Al atoms in the framework on the structure and activity of incorporated Fe species was performed using three NH_4-ZSM-5 samples of similar molar Si/Al ratio ~14, but dramatically different in the relative concentrations of Al pairs (Al–Si–Si–Al sequences in 6MRs) and single far distant Al atoms in the framework (Table 1). Samples containing 84% and 52% of framework Al atoms in Al pairs (denoted as Z-84 and Z-52, resp.) were kindly supplied by the Research Institute of Petroleum and Hydrocarbon Gases (Slovakia) and TRICAT (**TZP 302**), respectively; for analysis see Sections 2.2 and 3.1. The laboratory synthesized sample Z-20 was prepared as follows: 45.3 g of $Al(NO_3)_3{\cdot}9H_2O$ (Sigma–Aldrich) was dissolved in 150 ml of water, and 339 g of tetraethyl orthosilicate (TEOS, Sigma–Aldrich) was mixed with 75 ml of 100% ethanol, and the solutions were put together and stirred for 90 min at RT. Thereafter, 71.4 g of $NaNO_3$ (Sigma–Aldrich) in 200 ml of water was added under stirring. In the next step, 305.6 g of TPAOH (40% aqueous solution, Alfa Aesar) in 700 ml of water was added. The resulting mixture was stirred for 5 min, before transferring to a 2 l autoclave. Hydrothermal

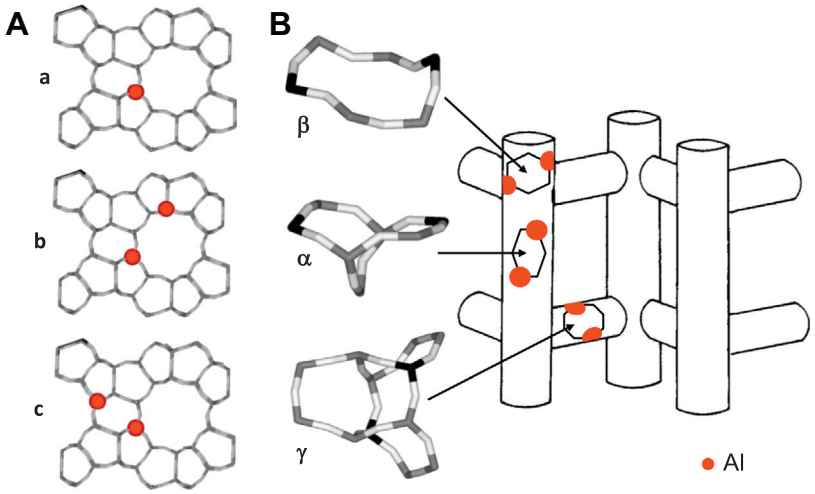

Fig. 1. Schematic illustration of the local arrangement of Al atoms in the ZSM-5 framework, based on analysis of the Co(II) ion-exchange capacity. (A) (a) Single far distant Al atoms (Al–O–(Si–O)$_{n>2}$–Al) able to compensate only monovalent ions. (b) Al unpaired (Al–O–(Si–O)$_{n>2}$–Al sequences in two 6MR rings) able to compensate the charge of solvated divalent [Co(H$_2$O)$_6$](II) complexes. (c) Al pairs (Al–O–(Si–O)$_{n=2}$–Al sequences in one 6MR ring) able to charge balance divalent bare Co(II) ions in dehydrated zeolites. (B) Locations of divalent bare Co(II) ions in α, β and γ sites in dehydrated zeolites.

Table 1
Characteristics of parent Na-ZSM-5.

Sample	Crystal size	Si/Al[a]	Si/Al$_{FR}$[b]	Co$_{max}$/Al[c]	Distribution of Al				
					Total Al[a]	Single Al[c]		Al pairs[c]	
	(μm)				(mmol g^{-1})	(mmol g^{-1})	(%)	(mmol g^{-1})	(%)
Z-20	~1	13.4	13.5	0.10	1.13	0.90	80	0.23	20
Z-52	~0.15	14.0	14.8	0.26	1.08	0.52	48	0.56	52
Z-84	~1	15.3	15.5	0.42	1.00	0.16	16	0.84	84

[a] From chemical analysis of Na-ZSM-5.
[b] From ^{29}Si MAS NMR spectra of Na-ZSM-5.
[c] From chemical analysis of Co(II) ion-exchanged parent zeolites or UV–Vis spectra of dehydrated Co(II)-ZSM-5.

synthesis was carried out at 250 rpm stirring and 170 °C for 6 days. After cooling down, the product was recovered by filtration and washed with deionized water.

All the zeolites were ion-exchanged with a 0.5 M $NaNO_3$ solution to obtain Na-ZSM-5 used for MAS NMR measurements. For analysis of the distribution of Al in the framework of the parent zeolites, part of the Na-ZSM-5 was further ion-exchanged to a maximum degree (three times) with 0.05 M Co(II) nitrate solution at RT and thoroughly washed with distilled water. Strict adherence to these conditions of Co(II) ion-exchange (Na-form, RT and 0.05 molarity) guaranteed the exclusive exchange of $[Co(II)(H_2O)_6]^{2+}$ ions adjacent to close Al atoms in hydrated Co-zeolites, which can be monitored by the characteristic Vis spectra of the $[Co(II)(H_2O)_6]^{2+}$ ions in the hydrated Co-ZSM-5 zeolites (spectra not shown; for details see [56,59]). The degree of exchange of the Co(II) hexaquo complexes represents the Co(II) ion-exchange capacity of the zeolite (Co$_{max}$ in Table 1). The other part of each Na-ZSM-5 sample was exchanged by a 0.5 M NH_4NO_3 solution (three times) to obtain NH_4-ZSM-5. The Si/Al composition and concentration of Co in the ZSM-5 zeolites were obtained by XRF analysis (accuracy ±3–5%) and are given in Table 1.

XRD (recorded by Bruker D8, Bruker AXS, USA) of all the samples exhibited the features of a ZSM-5 structure. The Na/Al ratios close to 1 and pore volumes of 0.13 cm^3 g^{-1} (determined from N_2 sorption at 77 K obtained on an ASAP2020 Micromeritics apparatus) indicated a well-developed crystalline structure (Supplement I). SEM images (JEOL JSM-5500LV) exhibited crystal sizes of about 1.0, 0.15, and 1.0 μm for Z-84, Z-52, and Z-20, respectively (see Supplement II). The homogeneous spatial distribution of Al throughout the zeolite crystals was supported by the Si/Al composition of the surface layer (up to 5 Å) similar to that (within 10%) of the bulk Si/Al. The MAS NMR spectra of the parent zeolites were measured on a Brucker Avance 500 MHz (11.7 T) Wide Bore spectrometer using ZrO_2 rotors with a rotation speed of 12 kHz. Comparison of the Si/Al composition obtained from chemical analysis and the ^{27}Al and ^{29}Si MAS NMR spectra indicated >95% of T$_d$-coordinated Al in the framework (chemical shift around 55 ppm); Oh-coordinated Al atoms (0 ppm) were not observed (Supplement III). The Si/Al composition corrected for the Al atoms in T$_d$ coordination (Si/Al$_{FR}$) was obtained from ^{29}Si MAS NMR analysis (Supplement IV) and is given in Table 1.

2.2. Analysis of the distribution of Al atoms in the framework of the parent ZSM-5

The distribution of framework Al atoms was analyzed by a well-developed methodology using Co(II) ions as probes to charge balance close Al atoms, supplemented by ^{27}Al and ^{29}Si MAS NMR analysis. The $[Co(II)(H_2O)_6]^{2+}$ ion-exchange capacity of hydrated Co-zeolites (Co$_{max}$) corresponded to Al atoms that were close enough to balance the charge of this Co hexaquo complex, and the concentrations of bare Co(II) ions at the α, β, and γ sites in dehydrated Co-zeolites coordinated exclusively to framework oxygen atoms (see Fig. 1, for details Ref. [55]) corresponded to two Al atoms localized in a single ring in the cationic sites.

As Si(2Si2Al) atoms were not found by ^{29}Si MAS NMR in any of the three parent ZSM-5 samples (see Supplement IV), Al–Si–Al sequences were not present in the framework, as commonly observed for ZSM-5 with Si/Al > 12 [51,53]; the detection limit of Si(2Si,2Al) atoms according to our experience with Si-rich zeolites

is estimated to be 2% of total Al (see also Ref. [60]). Therefore, the bare Co(II) ions coordinated to 6MRs of cationic sites are charge balanced only by Al–Si–Si–Al sequences (Al pairs), and the distribution of framework Al atoms in the parent ZSM-5 was calculated accordingly:

$$Al_{close} = 2xCo_{max} \quad (7)$$

$$Al_{single} = Al_{total} - 2xCo_{max} \quad (8)$$

$$Al_{pair} = 2x[Co_{\alpha} + Co_{\beta} + Co_{\gamma}] \quad (9)$$

$$Al_{unpair} = 2xCo_{max} - 2x[Co_{\alpha} + Co_{\beta} + Co_{\gamma}] \quad (10)$$

$$Al_{total} = Al_{pair} + Al_{single} + Al_{unpair} \quad (11)$$

where Co_{max} is the $[Co(II)(H_2O)_6]^{2+}$ ion-exchange capacity of hydrated ZSM-5, Co_{α}, Co_{β}, and Co_{γ} are the concentrations of bare Co(II) ions in the respective sites of dehydrated Co-ZSM-5, and Al_{total} is the concentration of framework Al atoms, Al_{close} is the concentration of Al atoms close enough to balance the $[Co(II)(H_2O)_6]^{2+}$ complex, Al_{pair} is the concentration of Al atoms in Al–Si–Si–Al sequences balancing bare Co(II) ions in dehydrated zeolites (reflecting in the d–d transitions), Al_{single} is the concentration of single Al atoms (Al–$Si_{n>2}$–Al sequences) occurring in different rings, and Al_{unpair} is the concentration of close Al atoms exchanging $[Co(II)(H_2O)_6]^{2+}$ ions and after dehydration yielding Co-oxo species, not bare Co(II) ions in cationic sites.

The Co_{max} was obtained from chemical analysis of the Co-zeolites. The concentrations of the bare Co(II) ions at the α, β, and γ sites were determined from quantitative analysis of the Vis spectra of the d–d transitions of the individual Co(II) ions deconvoluted to Gaussian bands and by using the extinction coefficients for the α, β, and γ types of Co(II) ions. Details of the analysis of the Vis spectra are described elsewhere [55]. The UV–Vis–NIR reflectance spectra of Co-ZSM-5 were recorded on a UV–Vis–NIR spectrometer equipped with a diffuse reflectance attachment using Spectralon® as a reference. The absorption intensities were expressed by the Schuster–Kubelka–Munk equation $\mathbf{F}(\mathbf{R}_{\infty}) = (1 - \mathbf{R}_{\infty})^2/2\mathbf{R}_{\infty}$, where $\mathbf{R}_{\infty}$ is the diffuse reflectance from a semi-infinite layer and $\mathbf{F}(\mathbf{R}_{\infty})$ is proportional to the absorption coefficient. The band positions of the individual bare Co(II) ions are determined in Ref. [55] for selected ZSM-5 samples with a highly predominating single type of Co(II) ions. The accuracy of the determination of the Co(II) ion-exchange capacity (Co_{max}) as well as of the sum of the concentrations of bare Co(II) ions was ±5%, as reported in detail in Ref. [56].

2.3. Preparation of Fe-ZSM-5 zeolites

A wide range of Fe concentrations from 0.39 up to 4.6 wt.% and Fe/Al 0.06–0.82 was prepared (Table 2) to investigate Fe-ZSM-5 samples containing both isolated Fe ions and Fe-oxo complexes, which are assumed to be active in N_2O decomposition and the NH_3-SCR-NO_x reaction. Iron was introduced into the three samples of dried parent NH_4-ZSM-5 zeolites (Z-20, Z-52 and Z-84) (Table 1) by ion-exchange using initial impregnation with an anhydrous solution of $FeCl_3$ in acetyl acetone. Fe-ZSM-5 samples were evacuated at 100 °C and then at 350 °C for 4 h. After thorough washing with distilled water, the Fe-samples were calcined overnight in a stream of air at 500 °C. Three series of Fe-ZSM-5 zeolites are listed in Table 2. The first number in, e.g. 1.5FeZ-20, means 1.5 wt.% of Fe in ZSM-5 containing 20% Al atoms in Al pairs. ^{57}Fe-ZSM-5 samples for Mössbauer spectroscopy measurements of different distributions of Al in the framework and about 1.5 wt.% ^{57}Fe were prepared by the same procedure using isotopically enriched $^{57}FeCl_3$.

Table 2
Composition of Fe-ZSM-5 zeolites and TOF and reaction rate r for NH_3-SCR-NO_x and decomposition of N_2O.

Sample	c_{Fe} (wt.%)	c_{Fe} (mmol g^{-1})	Fe/Al	NH_3-SCR-NO				Decomposition of N_2O			
				300 °C		350 °C		425 °C		450 °C	
				TOF ($s^{-1} \times 10^2$)	r (mol g^{-1} s$^{-1} \times 10^6$)	TOF ($s^{-1} \times 10^2$)	r (mol g^{-1} s$^{-1} \times 10^6$)	TOF ($s^{-1} \times 10^4$)	r (mol g^{-1} s$^{-1} \times 10^7$)	TOF ($s^{-1} \times 10^4$)	r (mol g^{-1} s$^{-1} \times 10^7$)
0.40FeZ-20	0.40	0.07	0.06					6.0	0.43	13.4	0.96
0.73FeZ-20	0.73	0.13	0.12	0.79	1.03	2.59	3.38	5.9	0.77	12.0	1.57
1.30FeZ-20	1.30	0.23	0.21	1.22	2.83	3.27	7.60	4.3	1.0	10.6	2.48
1.93FeZ-20	1.93	0.35	0.31	0.66	2.27	2.05	7.08	3.2	1.12	7.7	2.65
3.84FeZ-20	3.84	0.69	0.61	0.50	3.46	1.66	11.4				
0.39FeZ-52	0.39	0.07	0.06					11.1	0.77	26.3	1.84
0.81FeZ-52	0.81	0.15	0.13	0.87	1.26	2.56	3.72	11.3	1.64	28.9	4.19
1.22FeZ-52	1.22	0.22	0.20					7.4	1.62	19.0	4.16
1.64FeZ-52	1.64	0.29	0.27	0.43	1.26	1.34	3.94	5.5	1.62		
2.20FeZ-52	2.20	0.39	0.36	0.24	0.96	0.79	3.10	4.2	1.67	10.1	3.97
0.41FeZ-84	0.41	0.07	0.07	0.54	0.39	1.52	1.11	11.1	0.82	26.0	1.91
0.92FeZ-84	0.92	0.16	0.16	0.67	1.11	1.90	3.13	11.3	1.86	27.1	4.46
1.96FeZ-84	1.96	0.35	0.35	0.32	1.11	0.90	3.17	7.6	2.65	16.9	5.92
3.86FeZ-84	3.86	0.69	0.69	0.29	1.58	0.65	4.49				

2.4. Structure characterization of Fe species

Temperature-programmed reduction of Fe-ZSM-5 by hydrogen (H_2-TPR) was performed using an Altamira AMI-200 instrument. 100 mg of Fe-ZSM-5, placed in a quartz reactor, was dehydrated before the H_2-TPR measurement in a stream of air at 450 °C for 1 h, or followed by treatment in a stream of N_2O at 200 °C for 1 h, and then cooled to 35 °C. Reduction by hydrogen was carried out at a heating rate of 10 °C min^{-1} from 35 to 800 °C using a H_2/Ar stream (9.44 vol.% H_2) with a flow rate of 30 ml min^{-1}.

Mössbauer spectroscopic measurements were performed using self-supporting pellets (100 mg; diameter 8 mm) of ^{57}Fe-zeolites. The sample was placed in a laboratory-made device enabling transport between the heating region and the measuring position. Prior to recording the spectra, the sample was evacuated at 450 °C for 3 h or calcined in oxygen at 450 °C for 30 min, followed by brief evacuation for 3 min. The spectra were collected at RT on samples in a vacuum (10^{-3} Pa). The source of γ rays was ^{57}Co in a rhodium matrix and α-Fe foil was used as a reference. The spectra were deconvoluted into Lorentzian-shaped components using MossWinn software. Individual components were characterized by the isomer shift (IS) describing the oxidation state of the Fe species and quadrupole splitting (QS) related to the Fe coordination. The Mössbauer spectra of the Fe-zeolites could also contain a magnetic component arising from mutually interacting Fe(III) species, characterized by the isomer shift and magnetic hyperfine field (B_{fh}). The assignment of the Mössbauer parameters to Fe species in Fe-ZSM-5 was based on the previously established analysis given in Refs. [26,28,61].

2.5. Catalytic reactions of N_2O decomposition and NH_3-SCR-NO_x

N_2O decomposition was carried out using a fixed-bed plug flow-through micro-reactor in the temperature range 300–450 °C. 100 mg of the catalyst in a U-shaped reactor was pre-treated in a helium stream at 450 °C for 2 h and then in an oxygen stream at 450 °C for 1 h. The feed contained 1000 ppm N_2O in He with a total flow rate of 300 ml min^{-1}, corresponding to GHSV 90,000 h^{-1}. The analysis of N_2O/NO_x, N_2 and O_2 gas compositions at the reactor outlet was performed using an Advanced Optima (ABB) IR analyzer (N_2O), chemiluminescence NO_x analyzer AH (MLU) and Hewlett Packard 5890 II gas chromatograph. The mass balance of N_2 and O_2 was achieved. Concentration of NO_x in the reactor outlet was below 1 ppm. The reproducibility in N_2O conversion was ±0.2%.

The NH_3-SCR-NO reaction was monitored in a quartz tubular down-flow reactor with a thermocouple placed in the center of the catalyst bed. The reactant gases (NO, NH_3, and O_2) and the carrier gas (He) were fed from independent mass flow controllers. All the reactor lines were tempered at 180 °C to prevent the formation of NH_4NO_3. The reactor was heated to an initial temperature of 500 °C and the concentration of reactants and products was read stepwise at steady state at a reaction temperature from 500 to 200 °C. NO, NO_2, and NH_3 were analyzed using a UV photometric analyzer (ABB AO2000-Limas11UV), and N_2O was determined with an infrared absorption photometer (ABB Uras26 EL3020). The experimental conditions for the SCR reaction were as follows: total gas flow 350 cm^3 min^{-1} and weight of catalysts 20.5 mg corresponding to GHSV ~510,000 h^{-1}; NO, 490 ppm; NH_3, 520 ppm; O_2, 2%; balance He. In these studies, NO_x conversion is defined as the reduction of NO and NO_2 to N_2. In all cases, the concentration of N_2O in the products was <2 ppm. The reproducibility in NO_x conversion was ±2%.

The kinetic regime under the reaction conditions was confirmed for both reactions. The same conversions in N_2O decomposition were attained with catalyst weights from 30 to 100 mg and total flow rates from 100 to 333 ml min^{-1}, equal to GHSV 90,000 h^{-1}. With SCR-NO_x at GHSV 510,000 h^{-1}, the catalyst weights of 20.5 and 15.0 mg and flow rates of 350 and 256 cm^3 min^{-1}, gave identical yield of N_2. The crystal sizes of parent zeolites ⩽1 μm (see Table 1) guaranteed the absence of intra-crystalline diffusion constrains, as showed in our preceding study for Fe-ZSM-5 with crystal size up to 2.5 μm [26], and also reported for crystals <2 μm [62–65].

The rates of N_2O decomposition to N_2 and O_2, and SCR-NO_x to N_2 per gram of catalyst (mol $g_{catalyst}^{-1}$ s^{-1}) were calculated from the conversions and yields, respectively, by using pseudo-first-order kinetic equation, in agreement with the reported reaction rate orders with respect to N_2O [63,66–68] and NO [27,69–71], both equal to 1. Oxygen has negligible effect on the N_2O decomposition over Fe-ZSM-5 [72]. At NH_3-SCR-NO_x ammonia as well as water exhibit zero order [27,67–69]. Changes in oxygen concentration do not significantly affect the reaction rate, as it is present in a high excess. Hence, the rate equation can be written as $r = F/W^*(-\ln(1-x))$ where F is the flow rate of the feed (mol of N_2O or NO per s^{-1}) and W is the weight of the catalyst (g). The turn-over-frequencies TOF_{N_2O} (mol_{N_2O} mol_{Fe}^{-1} s^{-1}) and TOF_{SCR} (mol_{N_2} mol_{Fe}^{-1} s^{-1}) were expressed in terms per total Fe. The apparent activation energies and the pre-exponential factors were estimated from the Arrhenius plots.

3. Results

3.1. Distribution of Al atoms in the framework of parent ZSM-5 zeolites

Si(2Si2Al) atoms were not found by ^{29}Si MAS NMR (Supplement IV) in the parent ZSM-5, reflecting the absence of Al–Si–Al sequences in the framework. Therefore, the nearest Al atoms in the framework could be Al–Si–Si–Al sequences (Al pairs) located in 6MRs, but not in 5MRs.

The concentrations of single Al atoms are represented by the differences between the concentrations of Al atoms in the framework and twice the Co_{max} exchange capacity of the hydrated Co-zeolites (Eq. (7)). The concentrations of bare Co(II) ions at α, β, and γ sites in dehydrated Co-ZSM-5 (see Fig. 1) were obtained from quantitative analysis of the intensities of the d–d absorptions in the UV–Vis spectra depicted in Fig. 2. The Vis absorptions of bare Co(II) ions in dehydrated Co-ZSM-5 zeolites ranging from 14,000 to 23,000 cm^{-1} were deconvoluted into the seven bands (see Fig. 2 illustrating the deconvolution) of the three types of bare Co(II) ions coordinated with the α-, β-, and γ-type framework rings (see Fig. 1, and for details Ref. [55]) charge balanced by Al pairs located in these framework rings.

As the $[Co(II)(H_2O)_6]^{2+}$ ion-exchange capacity of hydrated Co-zeolites (Co_{max}) corresponded (within 5 rel.%) to the sum of the concentrations of bare Co(II) ions in the α, β, and γ sites for all three ZSM-5 samples, the concentrations of close Al atoms in different rings (Al_{unpair}, Eq. (10)) were negligible and well below 5% of total Al, and therefore, it was neglected. In agreement with this finding, the UV–Vis spectra of the individual Co-ZSM-5 (Fig. 2) contained only very low intensity of the broad CT absorption around 30,000 cm^{-1}, corresponding to Co-oxo species formed from $[Co(II)(H_2O)_6]^{2+}$ ions exchanged adjacent to unpaired Al atoms; note that the extinction coefficients of the CT transitions of Co-oxo species were estimated to be approximately 50 times higher compared to those of the d–d transitions of Co(II) ions [59].

Summing up, the quantitative analysis of counter Co(II)-ion probes for the distribution of negatively charged AlO_4^- in the framework of the ZSM-5 samples (Eqs. (7)–(11), Table 1) showed that the parent ZSM-5 samples (Z-20, Z-52, and Z-84) exhibited different populations of two predominant Si–Al arrangements in the framework: (i) Al–Si–Si–Al sequences (denoted as Al pairs)

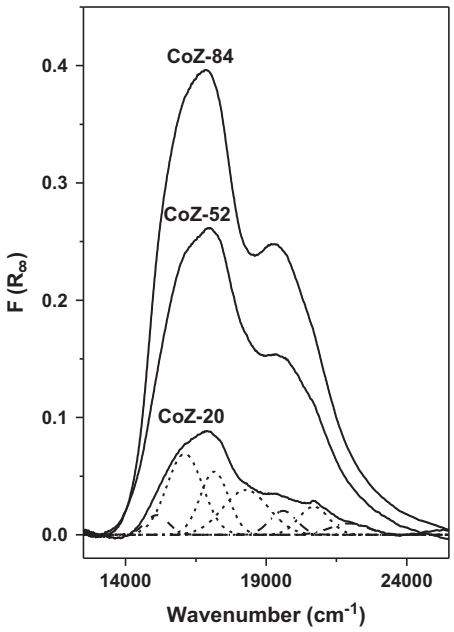

Fig. 2. Diffuse reflectance Vis spectra of dehydrated Co(II)-ZSM-5 zeolites used for analysis of the population of Al pairs (Al–O–(Si–O)$_{n=2}$–Al sequences in one 6MR ring able to charge balance divalent bare Co(II) ions in dehydrated zeolites).

located in 6MRs of the α-, β-, and γ-type of cationic sites, and (ii) single far distant Al atoms in Al–Si$_{n>2}$–Al sequences occurring in any different, so-far not specified, framework rings. The Al pairs were mostly (approx. 60%) located in the β-type 6MRs at the intersection of the straight and sinusoidal channel, followed by their location (approximately 40%) at the α-type 6MRs on the wall of the straight channel, while their location at the γ-type boat shape site in the sinusoidal channel was very low (<10%); cf. Fig. 1.

3.2. TPR-H_2

Fig. 3A compares H_2-TPR profiles at increasing Fe concentrations for FeZ-20 and FeZ-84 series (pre-treated in the air at 450 °C) exhibiting low and high populations of Al pairs in their framework. The Fe(II) ions present in all the Fe-ZSM-5 samples pre-treated in oxygen at 450 °C (demonstrated by Mössbauer analysis in Section 3.3, Table 4) are known to be highly stabilized in zeolites and are not reduced by hydrogen up to 700 °C [26]. Therefore, the monitored hydrogen consumption at increasing temperature reflects reduction of only Fe(III)-oxo species. Single bare Fe(III) ions cannot be coordinated with the framework rings because of insufficient negative AlO_4^- charge (absence of Al–Si–Al sequences) in 6 as well as 5MRs.

The reduction profiles in the 300–600 °C region were similar at low Fe contents (~0.4 wt.%) for the FeZ-20 and FeZ-84 series. At increasing Fe concentrations in the FeZ-84 series, a sharp dominant peak appeared at 390–400 °C, increasing with Fe loading, and only at high Fe content (4.6 wt.%, Fe/Al 0.82) was hydrogen also consumed in a broad range around 500 °C. The TPR profiles of the FeZ-20 series with prevailing single Al atoms in the framework differed in the appearance of a distinct low-temperature reduction shoulder starting from 250 °C with maximum at about 290 °C. This was accompanied by a shift of the main broad maximum of hydrogen consumption from 390 to 420–500 °C with increasing Fe content. Characteristic strong reduction at 390–400 °C observed with FeZ-84 was found with FeZ-20 only at high (4.6 wt.%, Fe/Al 0.82) Fe concentrations.

These results imply control of the distribution of Al atoms in the framework over the redox properties of the Fe species. The prevailing population of single Al atoms in the framework yielded a significant concentration of Fe(III)-oxo species of very high reactivity reduced at the lowest temperature, reflected in a broad shoulder appearing from 230 to 350 °C. Simultaneously, it was seen that the FeZ-20 series with predominating single Al atoms, in contrast to FeZ-84 with predominating Al pairs, yielded a higher population of difficult-to-reduce Fe(III)-oxo species reflected in a comparable Fe concentration in a broad range from 400 to 550 °C. We can currently speculate that these latter difficult-to-reduce Fe-oxo species can be connected with small Fe oxide particles with neutral charge, while the former highly reactive specific oligomeric species are charge balanced by single Al atoms.

The differences in the reduction of the FeZ-20 and FeZ-84 series with different populations of Al pairs in the framework were also

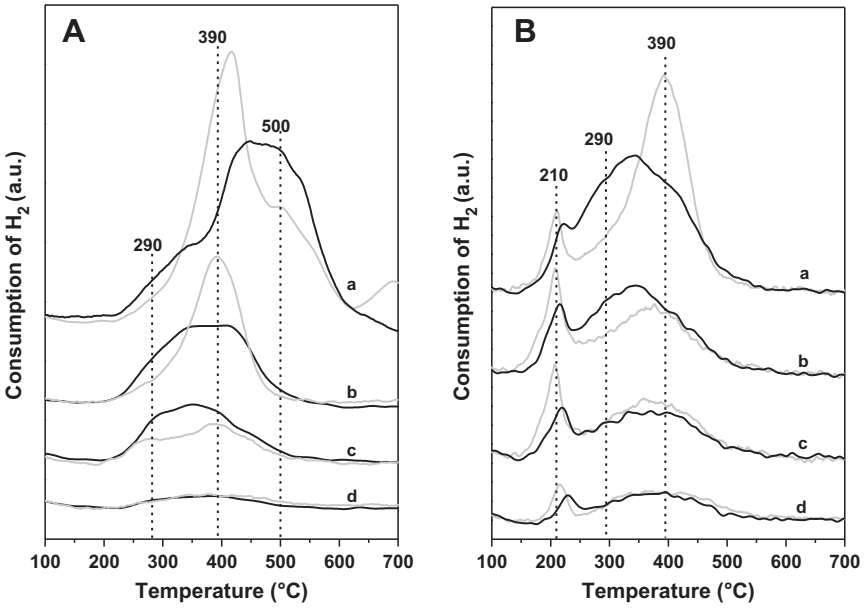

Fig. 3. Comparison of the H_2-TPR profiles of FeZ-20 (▬) and FeZ-84 (▬) with comparable Fe loadings, but differing in the distribution of Al atoms in the framework. (A) Fe-ZSM-5 zeolites pre-treated in the air at 450 °C. (a) 3.56FeZ-20 vs. 4.6FeZ-84; (b) 1.93FeZ-20 vs. 1.96FeZ-84; (c) 1.29FeZ-20 vs. 0.92FeZ-84; (d) 0.40FeZ-20 vs. 0.41FeZ-84. (B) Fe-ZSM-5 zeolites pre-treated in N_2O at 200 °C: (a) 1.93FeZ-20 vs. 1.96FeZ-84; (b) 1.29FeZ-20 vs. 1.02FeZ-84; (c) 0.73FeZ-20 vs. 0.92FeZ-84; (d) 0.40FeZ-20 vs. 0.41FeZ-84.

observed for the N_2O-pretreated zeolites at 200 °C (Fig. 3B). A new sharp reduction peak was observed at 210 °C for both series, but with significantly higher intensity for FeZ-84 compared to FeZ-20, and with the highest intensity for an Fe content of about 1–2 wt.% Fe. Simultaneously, the low-temperature shoulder ranging between 230 and 350 °C decreased in intensity, the sharp peak at 390–400 °C completely disappeared, and the reduction in a broad-temperature range originally at 400–550 °C shifted completely to a lower temperature. This indicates both the coordination of highly reactive atomic oxygen formed from N_2O decomposition to Fe(II) species and the general appearance of easily reducible Fe(III)-oxo species.

3.3. Mössbauer spectra

The Mössbauer spectra of the evacuated (at 450 °C for 3 h) ^{57}Fe-ZSM-5 with ~1.5 wt.% ^{57}Fe and Fe/Al ~ 0.25 and various populations of Al atoms in the Al pairs in the framework (ranging from 20 to 84 rel.%) as well as oxidized in oxygen at 450 °C together with their fits are shown in Figs. 4 and 5; their parameters and spectral contributions are listed in Tables 3 and 4. These treatments did not follow the conditions under which the N_2O decomposition and NH_3-SCR-NO_x reaction proceed, but were used to analyze the redox behavior of the Fe sites depending on the distribution of Al atoms in the framework. For high-spin Fe complexes coordinated with oxygen-containing ligands, i.e. those occurring in zeolites, the IS values for Fe(III) are lower compared to those for Fe(II). IS < 0.3 mm/s are assigned in the literature to Fe(III) in T_d coordination and those with IS > 0.3 mm/s to O_h coordination [61,73,74]. T_d-coordinated Fe(II) has IS 0.8–1.0 mm/s and QS around 1.0 mm/s, while higher QS is assigned to higher coordination numbers [75]. However, it is well known that, in pentasil ring zeolites (MFI, FER, BEA), those coordinations do not occur, but unusual coordination of metal ions definitely occurs far from those described above. Assignment of the individual spectral components presented here followed the previous analysis of the Mössbauer parameters of ^{57}Fe-ZSM-5 and ^{57}Fe-ferrierites of low concentration of Fe (Fe/Al ~ 0.1) described in Refs. [26,48,61]. For ^{57}Fe-ZSM-5 samples, the Fe/Al ~ 0.25 was chosen to possess various types of Fe species, as expected to be required for the reactions of N_2O decomposition and NH_3-SCR-NO_x.

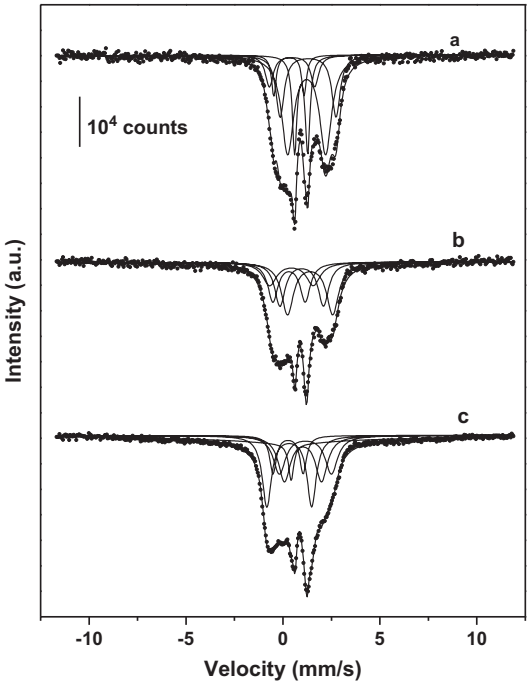

Fig. 4. Mössbauer spectra of ^{57}Fe-ZSM-5 (~1.5 wt.%) after evacuation at 450 °C for 3 h. (a) 1.5FeZ-84, (b) 1.5FeZ-52 and (c) 1.5FeZ-20. Spectra recorded at RT.

Deconvolution of the Mössbauer spectra of three ^{57}Fe-ZSM-5 samples (1.5 wt.% ^{57}Fe) dramatically differing in their populations of Al atoms in the Al pairs (from 20% to 84%) and the remaining single Al atoms led to five or six components with obtained high quality of spectra fitting. We were aware of the fact that using a high number of components for spectral fitting provides high flexibility in mathematical computations. Nevertheless, obtaining close IS and QS parameters for the individual samples encouraged us to ascribe the individual components to some Fe species, but at the same time, the obtained individual concentrations should be evaluated with great caution. The results of fitting were also supported by spectral parameters of Fe-ZSM-5 zeolites given in the literature [16,26,48,74,76,77].

Mössbauer spectrum of the dehydrated (evacuated) ^{57}FeZ-84 containing the highest concentration of Al pairs indicated that a prevailing part (82%) of the iron corresponds to divalent Fe(II) species. The D1 and D1A doublets with high QS values (IS 1.24 mm/s, QS 1.97 mm/s and IS 1.32 mm/s, QS 2.90 mm/s, respectively) indicate two different Fe(II) species with higher coordination numbers. They could be attributed to dinuclear counter $[Fe(II)–O–Fe(II)]^{2+}$ species and oligomeric Fe(II) species, respectively [26,48,77]. The D2 component (IS 0.96 mm/s, QS 0.67 mm/s) is assigned to bare Fe(II) ions in planar or close to planar coordination to 6MRs containing Al pairs (at β and α sites, see Fig. 1) [26,28,30]. The remaining Fe species (18%), described by components D3 and D4 (IS 0.33 and 0.49 mm/s) and the relatively high value of QS (1.55 and 2.35 mm/s, resp.) indicate two Fe(III)-oxo species of high coordination [28,30,48,61]. Bare Fe(III) ions coordinated exclusively to framework oxygen atoms cannot be present, because of the insufficient local negative charge (absence of 3 AlO_4^-) to balance them in 6MRs. The D3 component might be tentatively attributed to counter $Fe(III)O^+$ balanced by a single Al atom or more probably to dinuclear Fe(III)–μO_2–Fe(III) complexes, while the D4 component corresponded to O_h-coordinated Fe(III) in Fe(III)-oxo oligomers [26,28,30,48,61], probably connected with single Al atoms. A low but significant intensity of the relaxation S1 component (characterized by IS ~ 0.5 mm s^{-1} and B_{fh} > 40 T) was observed only for FeZ-20, indicating the presence (20%) of mutually interacting Fe(III) ions, as also reported in Ref. [74] and for Fe-zeolites in Refs. [26,48,61,76]. As the relaxation component appeared in auto-reduced Fe-ZSM-5 containing a lower population of Al pairs and, a higher population of single Al atoms, we assume that it probably originated from some oligomeric Fe(III)-oxo and/or small neutral Fe(III) oxide particles.

With the decreasing population of Al pairs and increasing population of single Al atoms in the framework of series FeZ-84, -52 and -20 (see Table 3), the sum of the relative concentrations of counter Fe(III)-oxo species, Fe(III)-oxo oligomers and small Fe(III) oxide particles (D4 + D5 + S1) increased from 18 through 34% to 53%.

Compared to auto-reduced ^{57}Fe-ZSM-5 in a vacuum at 450 °C (Table 4), the Mössbauer spectra of ^{57}FeZ-84 and ^{57}FeZ-20 calcined at 450 °C in oxygen (Fig. 5) showed a higher portion of Fe(III) for both samples, which increased from 18% to 50% and from 53% to 72%, respectively (Table 4). While the bare Fe(II) ions (D2) were not oxidized at 450 °C, the intensity of the D1 component decreased slightly and the D1A component completely disappeared. This implies marked differences in the redox behavior and thus the structure (including the local AlO_4^- surroundings) of Fe(II) species, reflected in the sequence of stabilization of divalence of Fe species corresponding to D2 > D1 > D1A components. Their redox behavior is in agreement with the character of these species and

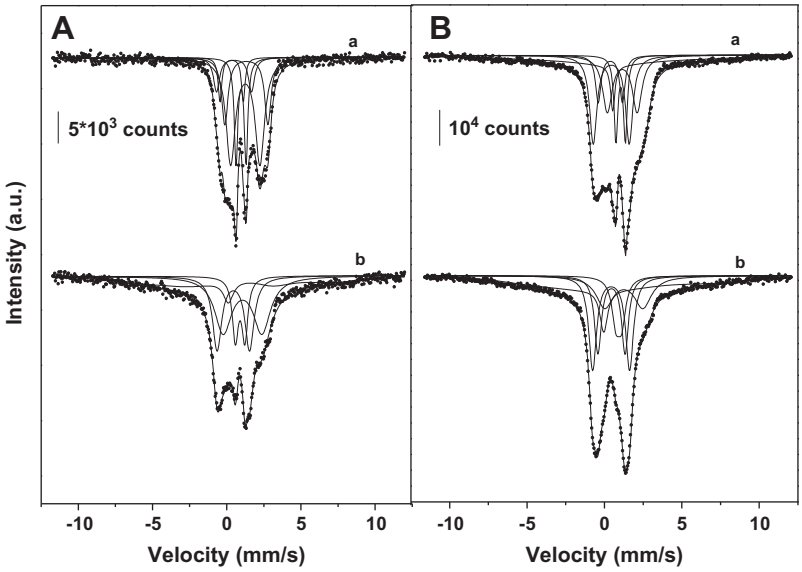

Fig. 5. Mössbauer spectra of ^{57}Fe-ZSM-5 (~1.5 wt.%) after (a) evacuation at 450 °C for 3 h, (b) O_2 oxidation at 450 °C for 30 min. (A) 1.5FeZ-84 and (B) 1.5FeZ-20. Spectra recorded at RT.

Table 3
Mössbauer parameters and spectral contribution of ^{57}Fe-ZSM-5 (~1.5 wt.% ^{57}Fe) with various Al distributions evacuated at 450 °C.

Zeolites	Component	IS (mm/s)	QS (mm/s)	B_{fh} (T)	Rel. (%)	Fe species	Fe(II)/Fe(III)
1.5FeZ-84	D1	1.24	1.97		45	$[Fe(II)–O–Fe(II)]^{2+}$	82/18
	D1A	1.32	2.90		20	Fe(II) oligomeric, O_h	
	D2	0.96	0.67		17	Bare Fe(II)	
	D3	0.33	1.55		8	$[Fe(III)O]^+$, Fe(III)–μO_2–Fe(III), O_h	
	D4	0.49	2.35		10	Fe(III) oligomers, O_h	
1.5FeZ-52	D1	0.96	2.25		29	$[Fe(II)–O–Fe(II)]^{2+}$	66/34
	D1A	1.40	2.33		22	Fe(II) oligomeric, O_h	
	D2	0.92	0.59		15	Bare Fe(II)	
	D3	0.31	1.66		16	$[Fe(III)O]^+$, Fe(III)–μO_2–Fe(III), O_h	
	D4	0.43	2.25		18	Fe(III) oligomers, O_h	
1.5FeZ-20	D1	1.03	2.01		19	$[Fe(II)–O–Fe(II)]^{2+}$	47/53
	D1A	1.15	2.70		16	Fe(II) oligomeric, O_h	
	D2	0.92	0.61		12	Bare Fe(II)	
	D3	0.26	1.61		10	$[Fe(III)O]^+$, Fe(III)–μO_2–Fe(III)	
	D4	0.33	2.32		23	Fe(III) oligomers, O_h	
	S1	0.50		48	20	Fe(III) oxides	

Table 4
Mössbauer parameters and spectral contribution of ^{57}Fe-ZSM-5 (~1.5 wt.% ^{57}Fe) treated in O_2 at 450 °C.

Fe-ZSM-5 +O_2	Component	IS (mm/s)	QS (mm/s)	B_{fh} (T)	Rel. (%)	Fe species	Fe(II)/Fe(III)
1.5FeZ-84	D1	1.04	2.28		36	$[Fe(II)–O–Fe(II)]^{2+}$	50/50
	D2	0.87	0.69		14	Bare Fe(II)	
	D4	0.42	2.21		25	Fe(III) oligomers, O_h	
	S1	0.5		42	25	Fe(III) oxides	
1.5FeZ-20	D1	1.30	2.04		16	$[Fe(II)–O–Fe(II)]^{2+}$	28/72
	D2	0.90	0.60		12	Bare Fe(II)	
	D3	0.44	1.67		19	$[Fe(III)O]^+$, Fe(III)–μO_2–Fe(III), O_h	
	D4	0.43	2.29		25	Fe(III) oligomers, O_h	
	S1	0.5		45	28	Fe(III) oxides	

related charge balance. Both the dinuclear $[Fe(II)–O–Fe(II)]^{2+}$ (D1) and even more the bare Fe(II) ions (D2) are highly stabilized against oxidation by molecular oxygen owing to their charge balance by Al pairs, while the oligomeric Fe(II) species (D1A), which can be oxidized to Fe(III)-oxo species, can be assumed to be less strongly bonded. It is worthwhile to mention that after the redox cycles (evacuation/oxidation) carried out at 450 °C the structure and population of the individual Fe species was not changed as observed by Mössbauer spectra.

It is summarized that, with the increasing relative concentration of Al pairs and decreasing that of single Al atoms in the ZSM-5 framework (at ~1.5 wt.% Fe), the concentration of Fe(II)

clearly increases and that of Fe(III)-oxo species decreases in both auto-reduced and oxidized Fe-ZSM-5. This finding provides evidence for high stabilization of bare Fe(II) ions by Al pairs in the 6MRs of cationic sites as well as dinuclear $[Fe(II)–O–Fe(II)]^{2+}$ entities. The increase in the concentration of Fe(III)-oxo species with increasing population of single Al atoms in the framework encourages us to connect at least these species with counter-ion complexes balanced by single Al atoms.

3.4. UV–Vis spectra

The UV–Vis spectra of the FeZ-20 and FeZ-84 series (evacuated at 450 °C) with low and high populations of Al pairs (and correspondingly high and low populations of single Al atoms) in the framework, respectively, as a function of Fe loading from 0.4 to 4.6 wt.% Fe (Fe/Al ~ 0.06 to 0.82) are shown in Fig. 6. Both series exhibited intense broad absorption starting from 25,000 to 50,000 cm^{-1} characterized by three maxima around 29,000, 39,000 and 47,000 cm^{-1}. These correspond to the O → Fe(III) ligand to metal charge transfer (LMCT) absorptions of Fe(III) species, while those of O → Fe(II) are expected at high energy above the 50,000 cm^{-1} range of the UV–Vis spectrometer, as the first O → Fe(II) CT band is shifted by at least 21,000 cm^{-1} to higher energy according to the Fe(II) and Fe(III) optical electronegativity [78]. Accordingly, all the observed absorptions originate from O → Fe(III) charge transfer transitions, albeit some contribution of O → Fe(II) CT transitions to the intensity cannot completely be excluded. Neither d–d transitions of the trigonal planar Fe(II) ions (7900 and 9600 cm^{-1}) reported for dehydrated Fe(II)-A type zeolite Refs. [79,80], nor bands of octahedral (8400 and 10,900 cm^{-1}, Refs. [79,80]) and square pyramidal (11,000 cm^{-1}, Refs. [79,80]) Fe(II)-aqua complexes were observed in the spectra of the dehydrated Fe-zeolites. Nevertheless, the presence of bare Fe(II) ions in cationic sites could be reflected in weak bands with maxima ranging within 5100–5600 cm^{-1}. These bands do not exhibit characteristic shape of combination vibration bands, and lie in the range of electronic transitions of high-spin four-coordinated Fe(II) complexes Refs. [79,80]. They can be attributed to approximately planar four-coordinated Fe(II) ions in the α and β sites. However, intensities of these bands are low, can be overlapped by various combination vibration bands, and they cannot be recommended without support of further experimental techniques as an unambiguous marker of the presence of Fe(II) ions in zeolites.

The broad absorptions with maxima at 47,000 and 39,000 cm^{-1} are connected with isolated Fe(III)-oxo species with T_d and O_h coordination [4]. The band at 29,000 cm^{-1} is attributed to dinuclear bridged or small defined polynuclear Fe(III)-oxo complexes [24,26,81]. The species of choice might be $Fe(III)O^+$ or dinuclear $[Fe(III)–\mu O_2–Fe(III)]^{2+}$. With increasing Fe loading in both Fe-ZSM-5 series, the intensity of the CT absorptions increased and the overall intensity of the FeZ-84 series was much lower compared to that of FeZ-20 at comparable Fe concentrations. Moreover, the absorptions of the FeZ-20 series are shifted to lower frequencies compared to FeZ-84. Assuming close extinction coefficients for LMCT, this indicates substantially more Fe(III) species present in series containing predominantly single Al atoms in the framework and their higher degree of oligomerization. At higher Fe loadings (>0.96 wt.% Fe), both the FeZ-20 and FeZ-84 series, exhibited in addition to the above described CT absorptions, a clear absorption edge at 18,500 cm^{-1} and a weak band at 12,000 cm^{-1}, assigned to small Fe oxide particles [17,80]. The more pronounced absorptions at 18,000 and 12,000 cm^{-1} were found with FeZ-20 compared to the FeZ-84 series, reflecting a higher concentration of small Fe oxide particles, because of the lower population of Al pairs able to balance divalent Fe complexes. These findings are in agreement with the Mössbauer spectral analysis (cf. Tables 3 and 4) indicating an increasing population of Fe(III)-oxo species (sum of D3, D4 and S1 components, Table 3) as the population of single Al atoms increases in the framework.

The above findings on the higher occurrence of Fe(II) cationic species with high population of Al pairs in the framework were also supported by the UV–Vis spectra of 1.5FeZ-20 and 1.5FeZ-84 oxidized in oxygen at 450 °C (Fig. 7). The LMCT absorptions of Fe(III)-oxo species showed an increase in intensity at 29,000 cm^{-1} and in a abroad range around 39,000 cm^{-1} after oxidation of the evacuated samples. Substantially higher increase in the intensity for the 1.5FeZ-84 sample implies much higher concentration of Fe(II) for higher population of Al pairs in the framework.

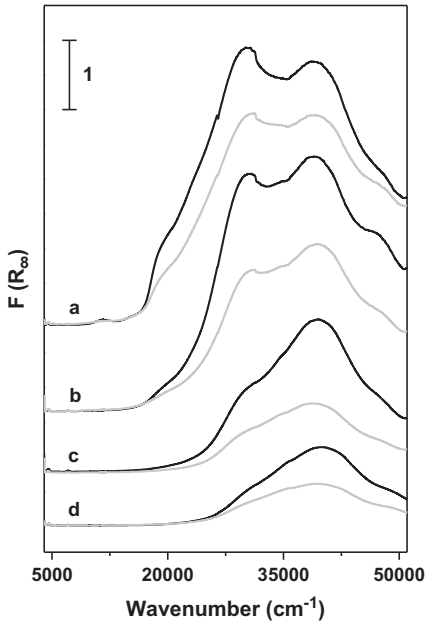

Fig. 6. Comparison of the diffuse reflectance UV–Vis–NIR spectra of FeZ-20 (▬) and FeZ-84 (▬) dehydrated under vacuum at 500 °C. (a) 3.56FeZ-20 vs. 4.6FeZ-84; (b) 1.93FeZ-20 vs. 1.96FeZ-84; (c) 0.73FeZ-20 vs. 0.92FeZ-84; (d) 0.40FeZ-20 vs. 0.41FeZ-84.

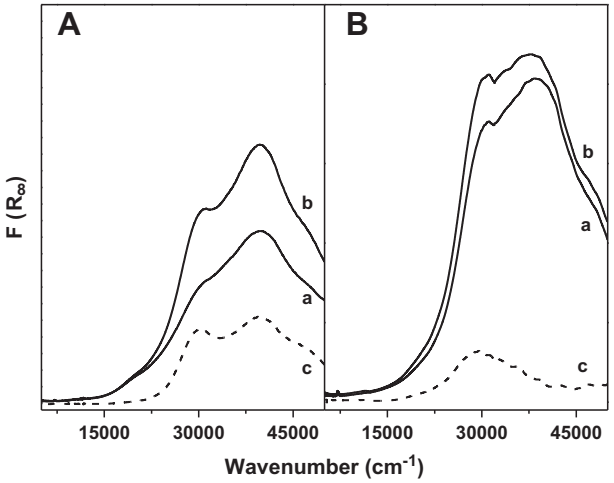

Fig. 7. UV–Vis spectra of ^{57}Fe-ZSM-5 (~1.5 wt.%) after (a) evacuation at 450 °C for 3 h, (b) O_2 oxidation at 450 °C for 30 min and (c) difference spectra. (A) 1.5FeZ-84 and (B) 1.5FeZ-20 with comparable Fe loadings, but differing in the distribution of Al atoms in the framework.

3.5. N_2O decomposition

Fig. 8A–C depicts temperature dependence of N_2O conversion, rates of N_2O decomposition to molecular products calculated from pseudo-first rate equation and the Arrhenius plots over the FeZ-20, -52 and -84 series, each depending on the Fe concentration; the reaction rates and turn-over-frequences (TOF_{N_2O}) at 425 and 450 °C are given in Table 2. In addition to an increasing Fe concentration, the increasing relative concentration of framework Al atoms in the Al pairs led to increased rate of N_2O decomposition. FeZ-84 zeolites exhibited more than twice the rates of N_2O decomposition compared to FeZ-20. While the rates of N_2O decomposition at 425 °C increased with increasing Fe concentration, TOF_{N_2O} values (per total Fe atom (s^{-1}), Table 2) were clearly higher at low Fe concentrations and for the Fe-ZSM-5 series with higher relative concentrations of Al pairs, as illustrated in Fig. 9 for samples with ~2 wt.% Fe. These results imply that the most active sites are preferentially occupied at low Fe loadings and in zeolites containing high population of Al pairs in the framework.

The apparent activation energies (Fig. 8C) for N_2O decomposition at 350–450 °C ranging from 114 to 140 kJ mol^{-1} are in agreement with those reported in the literature for N_2O decomposition over Fe(II)-ion-exchanged ZSM-5 (120–145 kJ mol^{-1} in Ref. [82] and 127–139 kJ mol^{-1} in Ref. [68]). The E_a values are higher for the most active (cf. conversion and rates in Fig. 8) FeZ-84 series (122–140 kJ mol^{-1}) compared to those of FeZ-20 (114–127 kJ mol^{-1}), but the former E_a values are compensated by ca two orders higher pre-exponential factor A ($\ln A \sim 15$ vs. 12). The high E_a values (195–215 kJ mol^{-1}) reported in Refs. [82–84] refer exclusively to the steamed Fe-ZSM-5 zeolites where Fe–Al–O species (not single Fe(II) ions) are assumed to be active sites. All these results clearly emphasize a dramatic effect of the structure and character of active Fe sites on the energetic parameters (free enthalpy and entropy) of catalytic N_2O decomposition.

The Fe(II)/Fe(III) ratio in the Fe-ZSM-5 series auto-reduced or calcined in oxygen at 450 °C (see Tables 3 and 4) and in an opposite sense the intensities of LMCT absorptions of monitored Fe(III) species can be related to both the activity in N_2O decomposition and

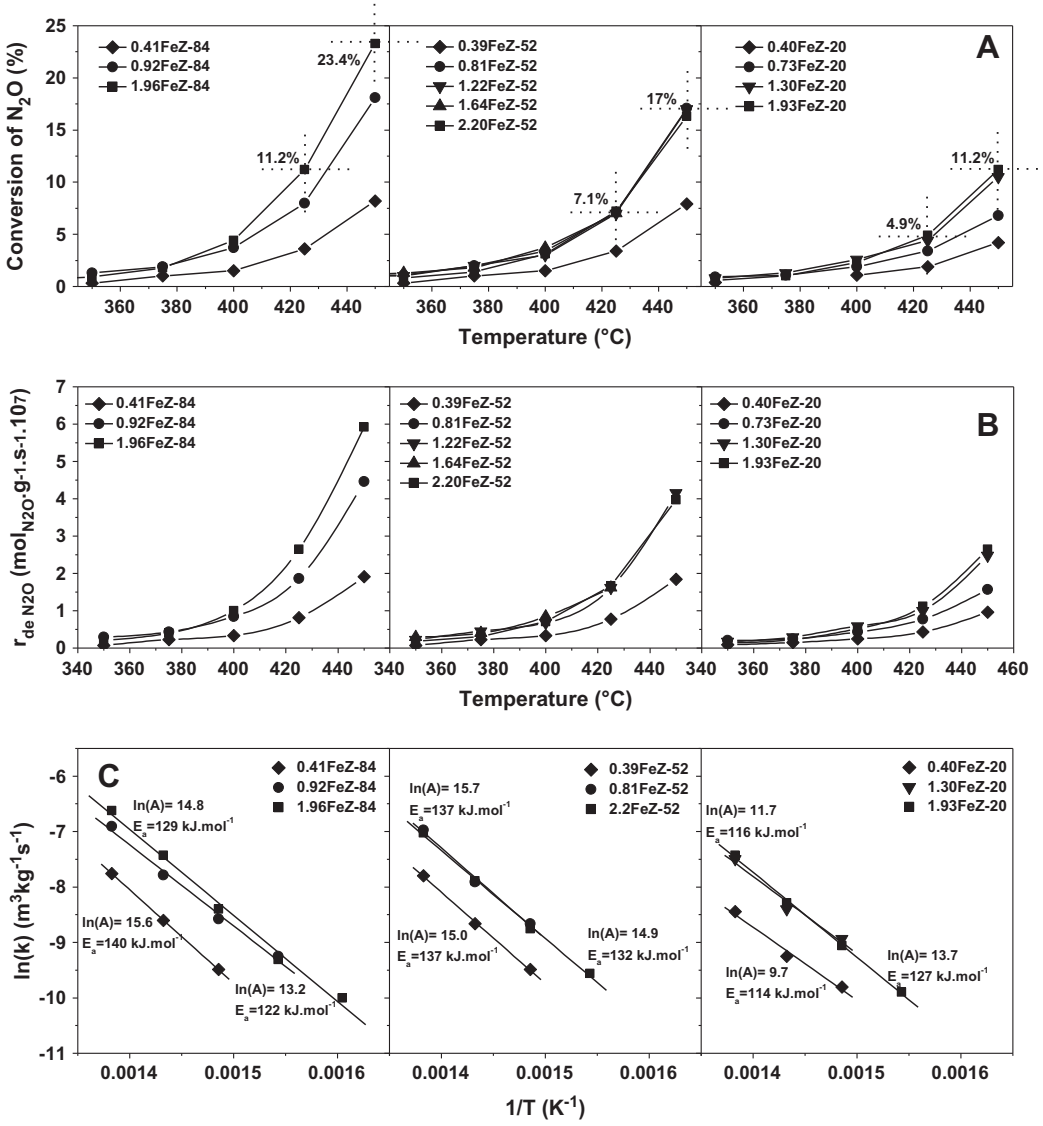

Fig. 8. Decomposition of N_2O over FeZ-84, FeZ-52 and FeZ-20 differing in the concentration of Al pairs in the zeolite framework. Reaction conditions: 1000 ppm N_2O in He, GHSV 90,000 h^{-1}. (A) Conversion of N_2O as function of temperature (The values of conversions for Fe-ZSM-5 with ~2 wt.% Fe at 425 and 450 °C are given in the figures.). (B) The reaction rate as a function of temperature assuming first-order kinetics. (C) The Arrhenius plot with determined the pre-exponential factors ln(*A*) and the activation energies.

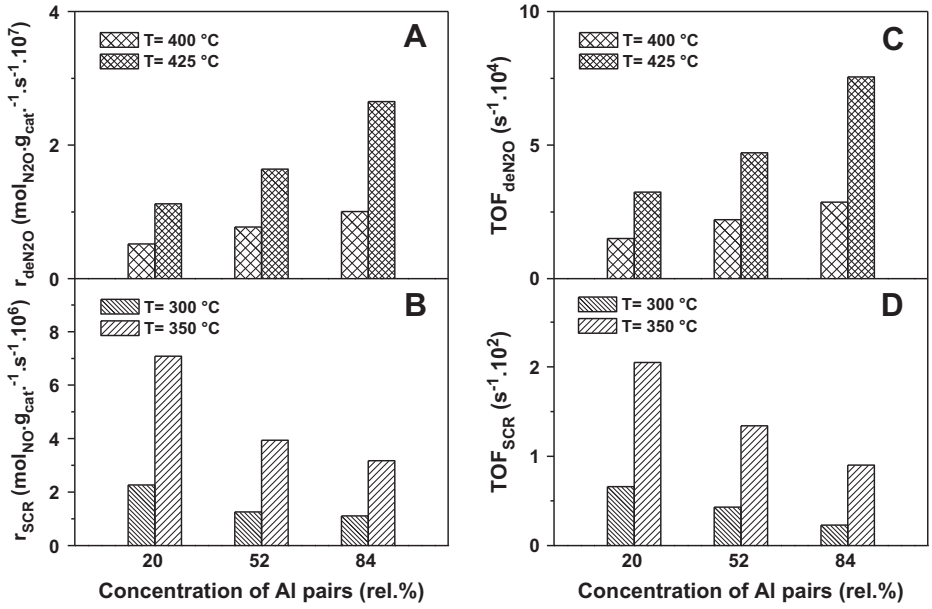

Fig. 9. Variation in (A), (B) reaction rate and (C), (D) turnover frequency for N_2O decomposition and NH_3-SCR-NO, respectively, over Fe-ZSM-5 (Fe ~ 2 wt.%) with concentration of Al pairs in the zeolite framework.

the presence of Al pairs in the framework. The increased population of Al pairs, leading to an increased population of Fe(II) species as well as TOF_{N_2O} per Fe, indicates that the most active sites are Fe(II) ions, in agreement with the recent conclusions of Dubkov et al. [48] and Kondratenko et al. [85], and our previous study [26]. At the same time, this finding indicates that the Al pairs give rise to preferential formation of Fe(II) species, the active sites in N_2O decomposition.

3.6. NH_3-SCR-NO_x

The effect of the distribution of framework Al atoms is also manifested in the conversion of NO in NH_3-SCR-NO, as shown in Fig. 10A in dependence on Fe concentration and temperature. The FeZ-20 series with higher concentration of single Al compared to FeZ-52 and FeZ-84 series exhibited markedly improved conversion of NO_x over the entire temperature range. This is the opposite trend compared to decomposition of N_2O, where the highest conversions were obtained over FeZ-84 series with the highest concentration of Al pairs. The rates of NO conversion to N_2 were calculated using pseudo-first-order kinetic equation assuming a first-order with respect to NO and zero-order with respect to NH_3 [27,69–71]. The reaction rates for NO conversion as a function of the reaction temperature (Fig. 10B) clearly demonstrate that the FeZ-20 series with higher concentration of single Al atoms exhibited more than twice the activity compared to FeZ-84 series. The SCR-NO_x rates per catalyst weight and TOF_{SCR} values per total Fe at 300 and 350 °C are given in Table 2. The TOF_{SCR} values depending on Al distribution in the framework for ~2 wt.% Fe are illustrated in Fig. 9. They clearly increase with the increasing population of single Al atoms in the Fe-ZSM-5 series. With increasing Fe concentration in the individual series, the TOF_{SCR} values first increased, followed by a decrease. Both these findings show that the active sites for SCR-NO_x cannot be exclusively Fe species predominantly occupied at low loadings and charge balanced by Al pairs, but rather sites occupied at intermediate loadings and increasing in concentration with increasing population of single Al atoms. The further decrease in TOF_{SCR} at higher Fe concentrations might be connected with the formation of small Fe oxide particles not resembling the character of counter ions. These are much less active as well as can contribute to the oxidation of ammonia to NO_x at high temperatures.

The Arrhenius plots of SCR-NO_x (Fig. 10C), albeit low number of data is presented, clearly showed two linear dependences of different slopes for each of three FeZ series. At temperatures 200–300 °C the activation energies ranged from ca 28 to 48 kJ mol^{-1}, while at 320–400 °C range they exhibited 64–81 kJ mol^{-1} These values well-agree with E_a = 36–51 kJ mol^{-1} published for the temperature range 200–300 °C [27,70] and 65–88 kJ mol^{-1} for temperatures 300–400 °C [27]. Although the integral conversions and TOF_{SCR} calculated from the pseudo-first-order rate equation showed higher activity of Fe species in FeZ-20 series, the E_a values for FeZ-20 series are the highest in both the temperature regions, but compensated by a higher pre-exponential A factor. Two different activation energies and pre-exponential factors for low and high temperature regions can be accounted for a change in a reaction mechanism and/or participation of different structure and concentration of Fe active sites. Brandenberger et al. [27] suggested at higher temperature contribution of Fe-oxo species of higher nuclearity to the SCR-NO_x reaction compared to single Fe ions presumably active at a lower temperature.

4. Discussion

Both the monoatomic bare Fe(II) ions coordinated only to framework oxygen atoms and dinuclear $[Fe(II)–O–Fe(II)]^{2+}$ complexes with an extra-framework oxygen atom, with their divalence stabilized even in an oxygen atmosphere in Fe-FER and Fe-MFI zeolites, have been indicated by Mössbauer analysis to be the most active sites for N_2O decomposition to molecular products [28,30,42,48,61]. On the other hand, from the NH_3-SCR-NO_x kinetics supported by qualitative UV–Vis analysis of the Fe(III) species, Brandenberger et al. [27] suggested isolated Fe(III)-oxo entities at 250 °C and from 350 °C dinuclear Fe(III)-oxo species as the most active, while Schwidder and Kumar et al. [3,86], assumed that oligomeric Fe-oxo species are the most active species. Although the real structure and coordination of these Fe active sites is still a matter of discussion, all these types of Fe species represent

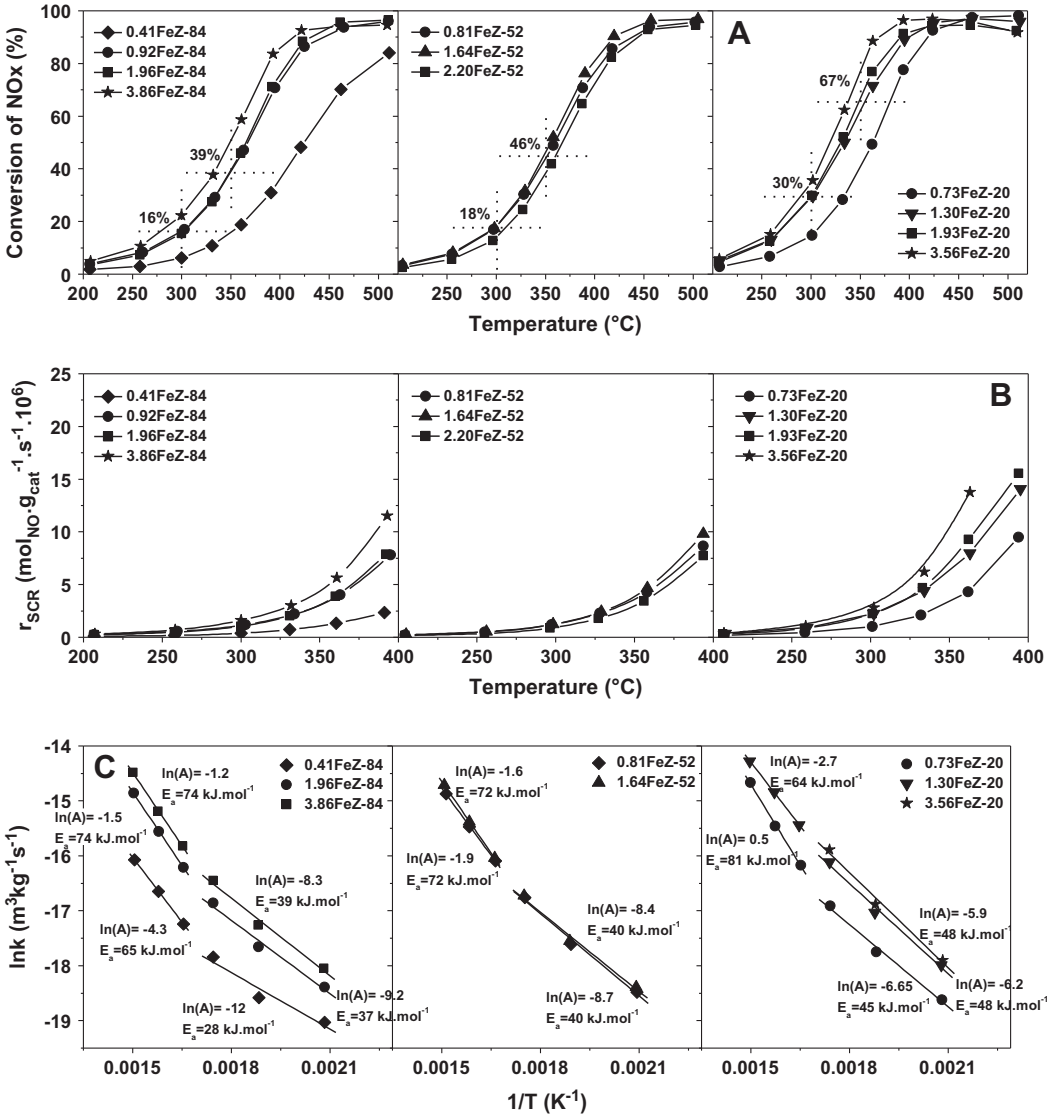

Fig. 10. NH_3-SCR-NO over FeZ-84, FeZ-52 and FeZ-20 differing in the concentration of Al pairs in the zeolite framework. Reaction conditions: 490 ppm NO, 520 ppm NH_3, 2% O_2 in He, GHSV 510,000 h^{-1}. (A) Conversion of NO_x as function of temperature (The values of conversions for Fe-ZSM-5 with ~2 wt.% Fe at 300 and 350 °C are given in the figures.). (B) The reaction rate as a function of temperature assuming first-order kinetics. (C) The Arrhenius plot with determined the pre-exponential factors ln(*A*) and the activation energies.

counter-ion species, and therefore species adjacent to a local negative charge of the framework.

4.1. Structures of Fe(II) and Fe(III) ion species related to the distribution of framework Al atoms

Ion-exchange involves two partners, the negatively charged framework (exhibiting local negative charges given by the distribution of AlO_4^-) and positively charged metal complexes exchanging into the zeolite. Compared to the Co(II) ion-exchange (if exclusively $[Co(II)(H_2O)_6]^{2+}$ is present), which can lead to complete quantitative occupation of the rings containing Al pairs by Co(II) ions (Co_{max}, Table 1), the Fe ion introduction is much more complex owing to the high variability in the Fe(II) and Fe(III) states and easy hydrolysis of both the Fe(III) and Fe(II) ions, with expected occurrence of mono-, di- or even polynuclear complexes in the exchanging media depending on the actual pH conditions inside the pores [23]. At low (<0.3 wt.%) Fe contents (see e.g. Ref. [3]) and Fe/Al < 0.1 in ZSM-5 and ferrierites [26,28,30] Fe(II) are predominantly located in cationic sites. Oligomeric products are also formed at higher Fe loadings and small Fe oxide particles were found in Fe-ZSM-5 prepared by CVD of $FeCl_3$ at high concentrations of Fe/Al 1 [24,34,78,87], in addition to counter Fe ions. In the latter cases, not all the Fe ions present are charge balanced by framework Al atoms.

While the concentrations of framework Al atoms in Al pairs and single Al atoms in the individual ZSM-5 samples in this study are specified, the structure of the Fe complexes occurring through ion-exchange using $FeCl_3$ in acetyl acetone with subsequent hydrolysis can only be speculated. The interaction of metal salts with NH_4- or H-zeolites at elevated temperatures is accompanied by the evolution of NH_4Cl or HCl [88] and here by exchange of $[Fe(III)Cl_2]^+$ and $[Fe(III)Cl]^{2+}$ ions, following their hydrolysis to $[Fe(III)(OH)_2]^+$ and $[Fe(III)(OH)]^{2+}$, respectively [89]. The hydroxylated Fe(III) complexes might be attached to the local negative charge of single Al atoms or Al pairs. Bare Fe(II) ions can be formed in ZSM-5 from $[Fe(III)OH^-]^{2+}$ balanced by Al pairs ($2AlO_4^-$) in 6MRs of cationic sites after their dehydration with participation of a proton of the framework SiOHAl. Similar to conditions in aqueous solutions, hydroxylated dinuclear $[Fe(III)–\mu O_2–Fe(III)]^{2+}$ complexes

might be formed inside the pores and exchanged adjacent to Al pairs of 6MRs. Under dehydration, they lost water molecules with the formation of $[Fe(II)–O–Fe(II)]^{2+}$ or $[Fe(III)–\mu O_2–Fe(III)]^{2+}$ entities. Such structure of Fe species coordinated to 6MRs of ZSM-5 was found feasible based on quantum chemical calculations [90].

The Mössbauer analysis of Fe(II) and Fe(III) structures (Tables 3 and 4) and UV–Vis spectra of Fe(III) species (Figs. 6 and 7) supplemented by information on the Fe(III) reduction in H_2-TPR (Fig. 3) exhibit (depending on the Fe concentration and population of Al pairs and single Al atoms) high variation in the concentrations of isolated single Fe ions, dinuclear and oligonuclear Fe species and, at high Fe loadings, small Fe oxide particles. A high portion of the Fe ions in Fe-ZSM-5 auto-reduced in a vacuum as well as those calcined in oxygen (both at 450 °C) appeared to be stabilized in a divalent state, as found for ^{57}Fe-ZSM-5 (~1.5 wt.% Fe, Fe/Al 0.25) and depending on the distribution of the framework Al atoms (Tables 3 and 4). This is in accordance with the results of the Panov group [48] and our previous study [26] reporting substantial occurrence of divalent Fe(II) in Fe-ZSM-5 oxidized by molecular oxygen. The increasing concentration of all types of monitored Fe(II) species (D1, D1A and D2 components in Table 3) in total from 47% to 82% (and *vice versa* decreasing concentration of Fe(III)-oxo species with an increasing population of Al atoms in Al pairs from 20% to 84%) indicates the decisive effect of the local negative framework charge of Al pairs on the bonding to and stabilization of a divalent state of counter Fe species in the zeolite.

For the three types of Fe(II) species, the D2 component (Table 3) of bare Fe(II), ranging from 12% to 17% of the total Fe species with increasing population of Al pairs, is ascribed to 4-fold coordination of bare Fe(II) ions with framework oxygens in the α and/or β sites of 6MRs. The most populated Fe(II) species are suggested to be dinuclear $[Fe(II)–O–Fe(II)]^{2+}$ (D1) coordinated to and charge balanced by an Al pair in 6MRs, from analogy with the dinuclear Fe complexes in methane monooxygenase as first suggested by Panov et al. [15,49,91]. Recent DFT calculations of energy characteristics reported by Li et al. [90] assuming coordination of dinuclear $[Fe(II)–O–Fe(II)]^{2+}$ complexes to various 6MRs containing Al pairs, indicate the feasibility of this bonding. The positive charges of these two types of Fe(II) species (single Fe and dinuclear species bound at cationic sites) is greatly affected by the high local negative charge imposed by Al pairs. Although they possess open coordination spheres, neither single Fe(II) ions nor part of the dinuclear complexes is oxidized by molecular oxygen at 450 °C, and a predominant part remains unchanged (cf. Tables 3 and 4). To the contrary, oligonuclear Fe(II) species of the D1A component (IS > 1.50 mm/s and QS > 2.30 mm/s) are readily oxidized by molecular oxygen to Fe(III)-oxo species. It follows that the bare Fe(II) and Fe(II)–O–Fe(II) species coordinated to 6MRs with Al pairs do not interact with di-oxygen, but both are oxidized by N_2O with the formation of highly reactive oxygen reflected by low-temperature reduction at 210 °C in H_2-TPR (Fig. 3). This highly reactive oxygen was described as a $Fe(III)–O^-$ radical anion detected by EPR [92]. Accordingly, three types of Fe species, differing markedly in their coordination to the framework and redox behavior, exhibit the following sequence in the stabilization of their divalent states: bare Fe(II) ions > $[Fe(II)–O–Fe(II)]^{2+}$ > oligomeric Fe(II) species.

In contrast to the Fe(II) species, the increasing concentration of the Fe(III)-oxo species and low concentration of Fe(III) oxide particles is connected with an increasing population of single Al atoms in the framework. It follows from the Mössbauer spectral analysis (Tables 3 and 4), the higher intensities of the UV–Vis spectra of Fe(III) ions and their red shift in FeZ-20 compared to the FeZ-84 series in the region from 50,000 down to 25,000 cm^{-1} corresponding to an increase in the population of polynuclear Fe(III)-oxo species compared to monomeric and dinuclear $[(Fe(III)–\mu O_2–Fe(III)]^{2+}$ species. Small Fe oxide particles appearing with Fe-ZSM-5 containing a predominant population of single Al atoms and, at higher Fe concentrations (absorption edge at 18,000 cm^{-1} in Fig. 6, the S1 magnetic component in Table 3) indicate a lack of sufficient local charge to balance the counter-ion species. The occurrence of a wide range of Fe(III) structures is also manifested in their different reducibility. The prominent H_2 reduction around 390–400 °C can be connected with Fe(III) entities balanced by Al pairs, probably $[(Fe(III)–\mu O_2–Fe(III)]^{2+}$ complexes, while the predominant population of single Al atoms in the framework also results in Fe(III)-oxo species with high potential to be reduced to Fe(II) by H_2 at low temperature (250–350 °C in Fig. 3). The readily reduced Fe-oxo species could be connected with $Fe(III)O^+$ charge balanced by single Al atoms, probably incorporated into the zeolite during the ion-exchange as $[Fe(III)(OH)_2^-]^+$ and/or specific Fe(III)-oxo species charge balanced by two single Al atoms in different rings. The high reactivity and thus low stability of FeO^+ is supported by DFT calculations of its energy characteristics [90]. But all these Fe-oxo structures exhibiting readily reduced extra-framework oxygens are associated with rings containing single Al atoms.

However, Mössbauer spectral analysis did not succeed in resolving the individual Fe(III) species, as they differed only in their quadrupolar splitting values, and also owing to the overlap with the intensity of the magnetic S1 component, reflecting the presence of interacting Fe(III) ions. Therefore, we consider only a general trend showing that the sum of the Fe(III)-oxo species increases with increasing population of single Al atoms in the framework. At least a predominant part of the Fe species preferring a trivalent state in the auto-reduced Fe-ZSM-5 is attached to single Al atoms.

Complete oxidation of all the Fe(II) sites to Fe(III) is feasible only by using N_2O, as shown by Dubkov et al. [48] and in our preceding study [26]. The $Fe(III)–O^-$ or Fe(IV)=O species supposed to be formed after oxidation of the Fe(II) sites by N_2O are very reactive, as follows from the lowest temperature (210 °C) of their reduction by hydrogen shown in Fig. 3.

4.2. Effect of the framework Al distribution and related Fe structures on the N_2O decomposition

It is well accepted that divalent Fe(II) sites are the active sites for N_2O decomposition over Fe-ZSM-5. This conclusion followed from the linear relationship between the concentration of Panov's α-sites, the Fe(II) ions adsorbing oxygen atoms from N_2O, and the rate of N_2O decomposition [1,48]. The assumed active Fe(II)–O–Fe(II) sites were suggested to originate from the dinuclear $[Fe(III)–\mu O_2–Fe(III)]^{2+}$ complexes. Later studies over low-loaded Fe-ferrierites (Fe/Al 0.03–0.1) supplemented with Mössbauer analysis of the coordination of Fe(II) ions have shown that the most active sites can also be isolated bare Fe(II) ions coordinated to 6MRs in cationic sites, as also supported by TOF_{N_2O} values decreasing with increasing Fe concentration in ZSM-5 (from trace concentrations of Fe in parent zeolites) [16,17,26,30,56]. This finding of decreasing TOF_{N_2O} with increasing concentration of Fe is also obtained here for all three series of Fe-ZSM-5 zeolites differing in the distribution of the framework Al atoms (Table 2). Moreover, TOF_{N_2O} also decrease in the individual Fe-ZSM-5 series at comparable Fe concentrations with decreasing population of the Al atoms in the Al pairs, as illustrated in Fig. 9 for temperatures of 400 and 425 °C. Both these dependences support the conclusion on the decisive positive effect of Al pairs in the zeolite framework for the formation of Fe(II) sites active in N_2O decomposition.

We have no information on the actual Fe(II)/Fe(III) valence state under the conditions of N_2O decomposition in the presence of molecular oxygen and NO_x intermediates (cf. Eqs. (1)–(3)). Even the concentrations of these molecular products and intermediates are low, the reaction atmosphere should be considered to be the

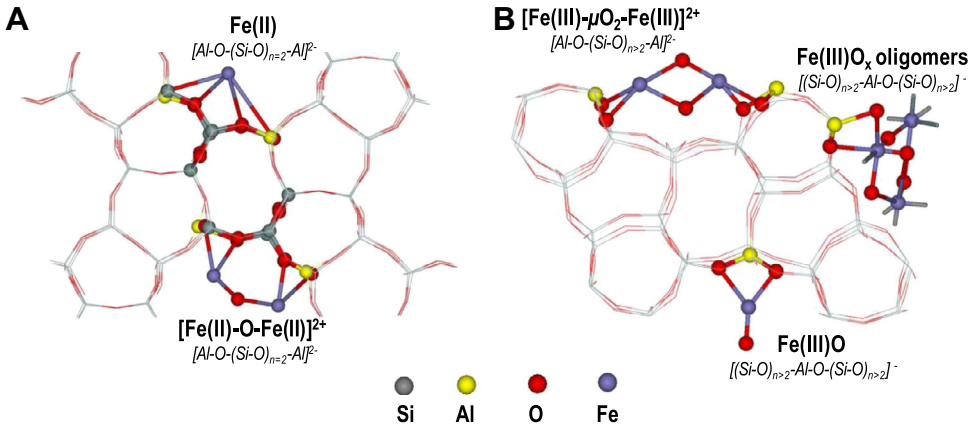

Fig. 11. Schematic illustration of main Fe species in the vicinity of (A) Al pairs (Al–O–(Si–O)$_{n=2}$–Al sequences in one 6MR ring) and (B) single far distant Al atoms (Al–O–(Si–O)$_{n>2}$–Al).

oxidizing agent. Nevertheless, following oxidation of auto-reduced Fe-ZSM-5 (of both series containing 20% and 84% of Al atoms in Al pairs, Table 4), the concentration of bare Fe(II) in cationic sites remained unchanged and only part of the [Fe(II)–O–Fe(II)]$^{2+}$ was oxidized. Thus, both the isolated Fe(II) and [Fe(II)–O–Fe(II)]$^{2+}$ ions charge balanced by Al pairs in the cationic sites are present and both represent the active sites for N_2O decomposition.

In addition to the observation that the most active sites are bare Fe(II) ions as well as dinuclear [Fe(II)–O–Fe(II)]$^{2+}$ complexes, the most important information is the observed decisive effect of the distribution of the Al atoms in the framework on the occurrence of isolated bare Fe(II) and [Fe(II)–O–Fe(II)]$^{2+}$ ion complexes and on the rate of N_2O decomposition. These are suggested to be (i) bare Fe(II) ions in α, β and γ cationic sites coordinated to 6MRs containing Al–Si–Si–Al sequences (Al pairs) and reflected as parameter D2 in the Mössbauer spectra and (ii) [Fe(II)–O–Fe(II)]$^{2+}$ entities coordinated to 6MRs containing an Al pair. Because of the highest population of Al pairs is located in the β-type 6MRs, the Fe(II) sites in both cases can be predominantly located at the intersection of the straight and sinusoidal channels. It is summarized that, by maximizing the population of Al pairs in the framework of ZSM-5, a maximum concentration of monoatomic Fe(II) and dinuclear [Fe(II)–O–Fe(II)]$^{2+}$ sites, the active sites for N_2O decomposition, can be obtained.

4.3. Effect of the framework Al distribution and related Fe structures on NH_3-SCR-NO_x

The complex NH_3-SCR-NO_x reaction, consisting of a number of reaction steps (cf. Eqs. (4)–(6)), is first order with respect to NO/NO_2 over Fe-ZSM-5 catalysts [27,50]. In general, enhancement of NO oxidation to NO_2 (with optimum NO/NO_2 = 1) increases the rate of di-nitrogen formation [12,93,94]. The rate order with respect to NH_3 is reported to be close to zero, with strong ammonia adsorption on Brønsted sites [95,96].

In contrast to the N_2O decomposition, the TOF_{SCR} per Fe for the individual Fe-ZSM-5 series at 300 °C at comparable Fe concentrations increases with increasing relative concentration of single Al atoms (Fig. 9). This indicates a relationship of the most active Fe sites to balancing of their charge by single Al atoms. Also within the individual Fe-ZSM-5 series, increasing TOF_{SCR} from low Fe loadings to a maximum value following its decrease with further increasing Fe concentration (Table 2) supports the relationship between the most active Fe sites and single Al atoms. These Fe sites might represent Fe-oxo species charge balanced by two single Al atoms located in different rings or balanced only by a single Al atom (see Fig. 11). This is not in contradiction with those findings of Iwasaki et al. [7], Brandenberger et al. [27] and Kumar et al. [86] reporting that the Fe-oxo species in the form of single Fe ions or oligomers of low nuclearity are the most active sites, particularly for SCR carried out above 300 °C. These Fe-oxo species are more readily oxidized at increasing temperature, as suggested also in Ref. [27], but there might also be a change in the reaction mechanism at around 315 °C reflected in the increase in the apparent activation energy from ca 28–48 kJ mol^{-1} to 64–81 kJ mol^{-1}.

The most important Fe species for NH_3-SCR-NO_x should exhibit a redox Fe(III)/Fe(II) cycle induced by molecular oxygen. These are definitely not bare Fe(II) ions coordinated to rings with Al pairs, as they are not readily oxidized by molecular oxygen, only by N_2O (see Fig. 3B). Participation of Fe(III)O$^+$ entities, although these might be formed after dehydration of the possibly present [Fe(III)(OH)$_2$]$^+$ attached to single Al atoms, is less probable based on the redox Fe(II)/Fe(III) cycle by molecular oxygen also because they presumably dimerize easy. As for the dinuclear Fe-oxo complexes, only those oxidized by molecular oxygen should be considered as the SCR active sites, not those active in N_2O decomposition. It follows that at least two types of di- or oligonuclear complexes should be present. The first one, assumed to be coordinated to 6MRs of cationic sites bearing Al pairs, represents an active site for N_2O decomposition and di- or oligonuclear Fe-oxo complexes are probably active in redox cycles with molecular oxygen taking place in SCR-NO_x. Those species highly active in NH_3-SCR-NO_x and charge balanced by a single Al atom might bear extra-framework oxygen(s) of high oxidation potential manifested in the low-temperature H_2-reduction around 250–300 °C (Fig. 3).

5. Conclusions

The heterogeneity of Fe-cationic species in Fe-ZSM-5 zeolites of different distributions of Al atoms in the framework has been investigated using Mössbauer, UV–Vis and H_2-TPR analysis of the structure and reactivity of Fe species. Three Fe-ZSM-5 zeolite series of similar Si/Al composition ~14 and with increasing Fe concentration, but differing in the relative concentrations of framework Al atoms in Al pairs (Al–Si–Si–Al sequences in 6MRs of cationic sites) and far distant Al atoms located in different rings, have been used to analyze the effect of the Al distribution on the structure of the Fe species and aim to tailor redox properties of Fe-ZSM-5. Investigation of the relevant structure and population of Fe-cationic species related to the Fe-ZSM-5 activity in reactions of N_2O decomposition and NH_3-SCR-NO revealed that:

(i) Fe-cationic species in Fe-ZSM-5 are predominantly represented by bare Fe(II) ions, dinuclear $[Fe(II)–O–Fe(II)]^{2+}$ and $[Fe(III)–\mu O_2–Fe(III)]^{2+}$ and Fe(III)-oxo species of low nuclearity.

(ii) The population of distinct cationic Fe species is largely directed by the local negative charge in the framework of ZSM-5 zeolites. High local negative charge in the framework originating from Al pairs in 6MRs led predominantly to the occurrence of bare Fe(II) and dinuclear $Fe(II)–O–Fe(II)^{2+}$ complexes, while a predominant population of single Al atoms caused in a comparable atmosphere a higher occurrence of trivalent Fe(III)-oxo species.

(iii) The stabilization of divalent Fe species by the charge of Al pairs in the framework ring decreased in the sequence: bare Fe(II) > $[Fe(II)–O–Fe(II)]^{2+}$ > oligonuclear Fe(II)–O, while readily reducible Fe(III)-oxo entities were charge balanced by single Al atoms.

(iv) The catalytic properties of these Fe-cationic species differ significantly and provided different activities in the decomposition of N_2O and for NH_3-SCR-NO_x. The most active sites in N_2O decomposition were found to be bare Fe(II) ions and dinuclear $[Fe(II)–O–Fe(II)]^{2+}$ complexes charge balanced by Al pairs. The most active sites in NH_3-SCR-NO_x were indicated to be Fe(III)-oxo species of low nuclearity attached to single Al atoms.

It can be concluded that the occurrence of framework Al atoms in Al–Si–Si–Al sequences (Al pairs) in the 6MRs of cationic sites and single Al atoms located in different rings dramatically affects redox behavior and catalytic activity of Fe counter species in ZSM-5. Presence of Al pairs in the zeolite framework highly stabilizes divalence of bare Fe(II) ions and dinuclear $[Fe(II)–O–Fe(II)]^{2+}$ complexes even in di-oxygen atmosphere by their charge compensation. These sites are oxidized only by N_2O and control the rate of N_2O decomposition. In contrast, the most active sites for NH_3-SCR-NO_x reaction are Fe(III)-oxo species of low nuclearity with their charge balanced only by single Al atoms in the framework. Partial compensation of the positive charge of Fe(III)-oxo species by the low local negative charge likely facilitates the Fe(III)/Fe(II) redox cycle involving molecular oxygen in an O_2-containing atmosphere and high catalytic activity in NH_3-SCR-NO_x.

Acknowledgments

This study was supported by the Czech Science Foundation (Project # P106/11/0624), by the Technology Agency of the Czech Republic (Project # TA01021377), and by RVO # 61388955.

Appendix A. Supplementary material

Supplementary data associated with this article can be found, in the online version, at http://dx.doi.org/10.1016/j.jcat.2014.01.019.

References

[1] G.I. Panov, V.I. Sobolev, A.S. Kharitonov, J. Mol. Catal. 61 (1990) 85–97.
[2] A. Uddin, T. Komatsu, T. Yashima, J. Chem. Soc., Faraday Trans. 91 (1995) 3275–3279.
[3] M. Schwidder, M.S. Kumar, K. Klementiev, M.M. Pohl, A. Bruckner, W. Grunert, J. Catal. 231 (2005) 314–330.
[4] S. Bordiga, R. Buzzoni, F. Geobaldo, C. Lamberti, E. Giamello, A. Zecchina, G. Leofanti, G. Petrini, G. Tozzola, G. Vlaic, J. Catal. 158 (1996) 486–501.
[5] R.W. Joyner, M. Stockenhuber, Catal. Lett. 45 (1997) 15–19.
[6] R.Q. Long, R.T. Yang, J. Catal. 194 (2000) 80–90.
[7] M. Iwasaki, K. Yamazaki, K. Banno, H. Shinjoh, J. Catal. 260 (2008) 205–216.
[8] M.S. Kumar, M. Schwidder, W. Grünert, A. Brückner, J. Catal. 227 (2004) 384–397.
[9] N. Hansen, A. Heyden, A.T. Bell, F.J. Keil, J. Phys. Chem. C 111 (2007) 2092–2101.
[10] R.Q. Long, R.T. Yang, J. Catal. 207 (2002) 224–231.
[11] I. Malpartida, O. Marie, P. Bazin, M. Daturi, X. Jeandel, Appl. Catal. B 113–114 (2012) 52–60.
[12] M.P. Ruggeri, I. Nova, E. Tronconi, Top. Catal. 56 (2013) 109–113.
[13] X. Feng, W.K. Hall, J. Catal. 166 (1997) 368–376.
[14] S. Brandenberger, O. Krocher, A. Tissler, R. Althoff, Ind. Eng. Chem. Res. 50 (2011) 4308–4319.
[15] V.I. Sobolev, G.I. Panov, A.S. Kharitonov, V.N. Romannikov, A.M. Volodin, K.G. Ione, J. Catal. 139 (1993) 435–443.
[16] K. Jisa, J. Novakova, M. Schwarze, A. Vondrova, S. Sklenak, Z. Sobalik, J. Catal. 262 (2009) 27–34.
[17] S. Sklenak, P.C. Andrikopoulos, B. Boekfa, B. Jansang, J. Novakova, L. Benco, T. Bucko, J. Hafner, J. Ddeek, Z. Sobalik, J. Catal. 272 (2010) 262–274.
[18] R.T. Yang, R.Q. Long, J. Catal. 188 (1999) 332–339.
[19] K. Krishna, M. Makkee, Catal. Today 114 (2006) 23–30.
[20] A. Grossale, I. Nova, E. Tronconi, Catal. Today 136 (2008) 18–27.
[21] R.Q. Long, R.T. Yang, J. Catal. 188 (1999) 332–339.
[22] A.Z. Ma, W. Grunert, Chem. Commun. (1999) 71–72.
[23] C.F. Baes, R.E. Mesmer, The Hydrolysis of Cations, Wiley, New York, 1976.
[24] G.D. Pirngruber, P.K. Roy, R. Prins, Phys. Chem. Chem. Phys. 8 (2006) 3939–3950.
[25] S. Brandenberger, O. Krocher, A. Tissler, R. Althoff, Appl. Catal. A 373 (2010) 168–175.
[26] P. Sazama, N.K. Sathu, E. Tabor, B. Wichterlova, S. Sklenak, Z. Sobalik, J. Catal. 299 (2013) 188–203.
[27] S. Brandenberger, O. Krocher, A. Tissler, R. Althoff, Appl. Catal. B 95 (2010) 348–357.
[28] E. Tabor, K. Zaveta, N.K. Sathu, A. Vondrova, P. Sazama, Z. Sobalik, Catal. Today 175 (2011) 238–244.
[29] J. Dedecek, L. Capek, P. Sazama, Z. Sobalik, B. Wichterlova, Appl. Catal. A 391 (2011) 244–253.
[30] Z. Sobalik, J. Novakova, J. Dedecek, N.K. Sathu, E. Tabor, P. Sazama, P. Stastny, B. Wichterlova, Microporous Mesoporous Mater. 146 (2011) 172–183.
[31] G. Berlier, G. Ricchiardi, S. Bordiga, A. Zecchina, J. Catal. 229 (2005) 127–135.
[32] D. Kaucky, Z. Sobalik, M. Schwarze, A. Vondrova, B. Wichterlova, J. Catal. 238 (2006) 293–300.
[33] M.S. Kumar, J. Perez-Ramirez, M.N. Debbagh, B. Smarsly, U. Bentrup, A. Bruckner, Appl. Catal. B 62 (2006) 244–254.
[34] E.M. El-Malki, R.A. Van Santen, W.M.H. Sachtler, Microporous Mesoporous Mater. 35–36 (2000) 235–244.
[35] J. Perez-Ramirez, F. Kapteijn, A. Bruckner, J. Catal. 218 (2003) 234–238.
[36] H. Guesmi, D. Berthomieu, L. Kiwi-Minsker, J. Phys. Chem. C 112 (2008) 20319–20328.
[37] I. Malpartida, E. Ivanova, M. Mihaylov, K. Hadjiivanov, V. Blasin-Aube, O. Marie, M. Daturi, Catal. Today 149 (2010) 295–303.
[38] M. Schwidder, M. Santhosh Kumar, A. Bruckner, W. Grunert, Chem. Commun. (2005) 805–807.
[39] A.A. Battiston, J.H. Bitter, W.M. Heijboer, F.M.F. De Groot, D.C. Koningsberger, J. Catal. 215 (2003) 279–293.
[40] A.A. Battiston, J.H. Bitter, D.C. Koningsberger, J. Catal. 218 (2003) 163–177.
[41] G.D. Pirngruber, P.K. Roy, N. Weiher, J. Phys. Chem. B 108 (2004) 13746–13754.
[42] E.J.M. Hensen, Q. Zhu, M.M.R.M. Hendrix, A.R. Overweg, P.J. Kooyman, M.V. Sychev, R.A. Van Santen, J. Catal. 221 (2004) 560–574.
[43] W.M. Heijboer, D.C. Koningsberger, B.M. Weckhuysen, F.M.F. De Groot, Catal. Today 110 (2005) 228–238.
[44] S.M. Maier, A. Jentys, E. Metwalli, P. Muller-Buschbaum, J.A. Lercher, J. Phys. Chem. Lett. 2 (2011) 950–955.
[45] W.M. Heijboer, A.A. Battiston, A. Knop-Gericke, M. Havecker, H. Bluhm, B.M. Weckhuysen, D.C. Koningsberger, F.M.F. De Groot, Phys. Chem. Chem. Phys. 5 (2003) 4484–4491.
[46] S.M. Maier, A. Jentys, M. Janousch, J.A. Van Bokhoven, J.A. Lercher, J. Phys. Chem. C 116 (2012) 5846–5856.
[47] J. Kim, A. Jentys, S.M. Maier, J.A. Lercher, J. Phys. Chem. C 117 (2013) 986–993.
[48] K.A. Dubkov, N.S. Ovanesyan, A.A. Shteinman, E.V. Starokon, G.I. Panov, J. Catal. 207 (2002) 341–352.
[49] G.I. Panov, V.I. Sobolev, K.A. Dubkov, V.N. Parmon, N.S. Ovanesyan, A.E. Shilov, A.A. Shteinman, React. Kinet. Catal. Lett. 61 (1997) 251–258.
[50] S. Brandenberger, O. Krocher, A. Tissler, R. Althoff, Catal. Rev. – Sci. Eng. 50 (2008) 492–531.
[51] J. Dedecek, Z. Sobalik, B. Wichterlova, Catal. Rev. – Sci. Eng. 54 (2012) 135–223.
[52] C.S. Cundy, P.A. Cox, Microporous Mesoporous Mater. 82 (2005) 1–78.
[53] P. Sazama, J. Dedecek, V. Gabova, B. Wichterlova, G. Spoto, S. Bordiga, J. Catal. 254 (2008) 180–189.
[54] J. Dedecek, V. Balgova, V. Pashkova, P. Klein, B. Wichterlova, Chem. Mater. 24 (2012) 3231–3239.
[55] J. Dedecek, D. Kaucky, B. Wichterlova, Microporous Mesoporous Mater. 35–36 (2000) 483–494.
[56] Z. Sobalik, P. Sazama, J. Dedecek, B. Wichterlova, Appl. Catal. A: Gen., in press. http://dx.doi.org/10.1016/j.apcata.2013.07.033.
[57] V. Gabova, J. Dedecek, J. Cejka, Chem. Commun. 9 (2003) 1196–1197.
[58] J. Dedecek, D. Kaucky, B. Wichterlova, Chem. Commun. (2001) 970–971.
[59] J. Dedecek, D. Kaucky, B. Wichterlova, O. Gonsiorova, Phys. Chem. Chem. Phys. 4 (2002) 5406–5413.
[60] C.A. Fyfe, G.C. Gobbi, J. Klinowski, J.M. Thomas, S. Ramdas, Nature 296 (1982) 530–533.
[61] E. Tabor, K. Zaveta, N.K. Sathu, Z. Tvaruzkova, Z. Sobalik, Catal. Today 169 (2011) 16–23.

[62] Q. Xiao, F. Yang, J. Zhuang, G. Qiu, Y. Zhong, W. Zhu, Microporous Mesoporous Mater. 167 (2013) 38–43.
[63] J. Perez-Ramirez, F. Kapteijn, J.C. Groen, A. Domenech, G. Mul, J.A. Moulijn, J. Catal. 214 (2003) 33–45.
[64] A. Shichi, A. Satsuma, T. Hattori, Appl. Catal. B 30 (2001) 25–33.
[65] A. Shichi, A. Satsuma, T. Hattori, Appl. Catal. A 207 (2001) 315–321.
[66] F. Kapteijn, G. Marban, J. Rodriguez-Mirasol, J.A. Moulijn, J. Catal. 167 (1997) 256–265.
[67] H. Xia, K. Sun, Z. Liu, Z. Feng, P. Ying, C. Li, J. Catal. 270 (2010) 103–109.
[68] P.K. Roy, G.D. Pirngruber, J. Catal. 227 (2004) 164–174.
[69] H.Y. Huang, R.Q. Long, R.T. Yang, Appl. Catal. A 235 (2002) 241–251.
[70] M. Iwasaki, K. Yamazaki, H. Shinjoh, Appl. Catal. A 366 (2009) 84–92.
[71] M. Devadas, O. Krocher, M. Elsener, A. Wokaun, N. Soger, M. Pfeifer, Y. Demel, L. Mussmann, Appl. Catal. B 67 (2006) 187–196.
[72] K. Sun, H. Xia, E. Hensen, R. van Santen, C. Li, J. Catal. 238 (2006) 186–195.
[73] R.L. Garten, W.N. Delgass, M. Boudart, J. Catal. 18 (1970) 90–107.
[74] E. Kuzmann, S. Nagy, A. Vertes, Pure Appl. Chem. 75 (2003) 801–858.
[75] R.G. Burns, Hyperfine Interact. 91 (1994) 739–745.
[76] L. Guczi, K. Lazar, React. Kinet. Catal. Lett. 96 (2009) 335–343.
[77] P. Guetlich, E. Bill, A.X. Trautwein, Mossbauer Spectroscopy and Transition Metal Chemistry Fundamentals and Applications Introduction, 2011.
[78] A. Zecchina, M. Rivallan, G. Berlier, C. Lamberti, G. Ricchiardi, Phys. Chem. Chem. Phys. 9 (2007) 3483–3499.
[79] J.P. Lange, K. Klier, Zeolites 14 (1994) 462–468.
[80] T. Grygar, J. Dedecek, P.P. Kruiver, M.J. Dekkers, P. Bezdicka, O. Schneeweiss, Catena 53 (2003) 115–132.
[81] L. Capek, V. Kreibich, J. Dedecek, T. Grygar, B. Wichterlova, Z. Sobalik, J.A. Martens, R. Brosius, V. Tokarova, Microporous Mesoporous Mater. 80 (2005) 279–289.
[82] G.D. Pirngruber, M. Luechinger, P.K. Roy, A. Cecchetto, P. Smirniotis, J. Catal. 224 (2004) 429–440.
[83] Q. Zhu, B.L. Mojet, R.A.J. Janssen, E.J.M. Hensen, J. Van Grondelle, P.C.M.M. Magusin, R.A. Van Santen, Catal. Lett. 81 (2002) 205–212.
[84] L.V. Pirutko, V.S. Chernyavsky, E.V. Starokon, A.A. Ivanov, A.S. Kharitonov, G.I. Panov, Appl. Catal. B 91 (2009) 174–179.
[85] E.V. Kondratenko, J. Perez-Ramirez, J. Phys. Chem. B 110 (2006) 22586–22595.
[86] M.S. Kumar, M. Schwidder, W. Grünert, U. Bentrup, A. Brückner, J. Catal. 239 (2006) 173–186.
[87] H.Y. Chen, W.M.H. Sachtler, Catal. Today 42 (1998) 73–83.
[88] H.G. Karge, B. Wichterlova, H.K. Beyer, J. Chem. Soc., Faraday Trans. 88 (1992) 1345–1351.
[89] L.J. Lobree, I.-C. Hwang, J.A. Reimer, A.T. Bell, J. Catal. 186 (1999) 242–253.
[90] G. Li, E.A. Pidko, R.A. Van Santen, C. Li, E.J.M. Hensen, J. Phys. Chem. C 117 (2013) 413–426.
[91] V.S. Chernyavsky, L.V. Pirutko, A.K. Uriarte, A.S. Kharitonov, G.I. Panov, J. Catal. 245 (2007) 466–469.
[92] E. Berrier, O. Ovsitser, E.V. Kondratenko, M. Schwidder, W. Grunert, A. Bruckner, J. Catal. 249 (2007) 67–78.
[93] M. Colombo, I. Nova, E. Tronconi, V. Schmeißer, B. Bandl-Konrad, L. Zimmermann, Appl. Catal. B 111–112 (2012) 106–118.
[94] M. Schwidder, S. Heikens, A. De Toni, S. Geisler, M. Berndt, A. Brückner, W. Grünert, J. Catal. 259 (2008) 96–103.
[95] S. Brandenberger, O. Kröcher, A. Wokaun, A. Tissler, R. Althoff, J. Catal. 268 (2009) 297–306.
[96] M. Colombo, G. Koltsakis, I. Nova, E. Tronconi, Catal. Today 188 (2012) 42–52.